Microtubule-dependent Plus- and Minus End–directed Motilities Are Competing Processes for Nuclear Targeting of Adenovirus

Maarit Suomalainen, Michel Y. Nakano, Stephan Keller, Karin Boucke, Robert P. Stidwill, and Urs F. Greber

Institute of Zoology, University of Zürich, CH-8057 Zürich, Switzerland

Abstract. Adenovirus (Ad) enters target cells by receptor-mediated endocytosis, escapes to the cytosol, and then delivers its DNA genome into the nucleus. Here we analyzed the trafficking of fluorophore-tagged viruses in HeLa and TC7 cells by time-lapse microscopy. Our results show that native or taxol-stabilized microtubules (MTs) support alternating minus- and plus end–directed movements of cytosolic virus with elementary speeds up to 2.6 μm/s. No directed movement was observed in nocodazole-treated cells. Switching between plus- and minus end–directed elementary speeds at frequencies up to 1 Hz was observed in the periphery and near the MT organizing center (MTOC) after recovery from nocodazole treatment. MT-dependent motilities allowed virus accumulation near the MTOC at population speeds of 1–10 μm/min, depending on the cell type. Overexpression of p50/dynamitin, which is known to affect dynein-dependent minus end–directed vesicular transport, significantly reduced the extent and the frequency of minus end–directed migration of cytosolic virus, and increased the frequency, but not the extent of plus end–directed motility. The data imply that a single cytosolic Ad particle engages with two types of MT-dependent motor activities, the minus end–directed cytoplasmic dynein and an unknown plus end–directed activity.

Key words: adenovirus • virus entry • microtubules • bidirectional movement • dynein/dynactin

Viruses which replicate in the cell nucleus must target their genome to the nucleus when entering a new host cell. One of the obstacles these viruses encounter is the diffusional barrier imposed by the cytoplasm. Within the eukaryotic cytoplasm organelles, solutes, and a complex lattice-like mesh of microtubule (MT),[1] actin, and intermediate filament networks effectively restrict free diffusion of molecules larger than 500 kD (Luby-Phelps, 1994; Seksek et al., 1997). Movement of large complexes, like membranous organelles and also ribonucleoprotein particles in developing oocytes is dependent on active processes and generally involves either the actin or MT cytoskeleton (Grünert and St. Johnston, 1996; Hirokawa et al., 1998; Holleran et al., 1998; Mermall et al., 1998). Similarly, viral structures destined for nuclear delivery can be large complexes up to hundreds of nanometers in diameter, and are thus not expected to move by free diffusion through the cytoplasm, but engage with some form of active transport (Greber, 1998a; Whittaker and Helenius, 1998). A known form of cell-assisted pathogen movement is the actin polymerization-dependent motility of cytosolic *Vaccinia* virus and *Shigella* and *Listeria* bacteria (Cudmore et al., 1997; Ireton and Cossart, 1997; Welch et al., 1997). Examples for MT-dependent processes are the movement of endosomal *reovirus* (Georgi et al., 1990) and the localization of cytosolic Herpes simplex virus capsids to the cell nucleus (Sodeik et al., 1997).

Human adenoviruses (Ads) are nonenveloped viruses, which replicate and produce progeny virions within the nucleus of an infected cell, i.e., epithelial cells of the upper and lower respiratory tract, or the gastrointestinal and urinary tracts (for reviews see Horwitz, 1990; Shenk, 1996). The virus particle is icosahedral, has a diameter of ~90 nm, and is composed of an outer capsid and an inner DNA-associated core with a 36-kb linear DNA, two terminal proteins, and condensing proteins V and VII (Burnett, 1997). Ads, such as the common type 2 or 5 viruses (Ad2

M. Suomalainen and M.Y. Nakano contributed equally to this work.

Address correspondence to U.F. Greber, Institute of Zoology, University of Zürich, Winterthurerstrasse 190, CH-8057 Zürich, Switzerland. Tel.: (41) 1 635 4841. Fax: (41) 1 635 6822. E-mail: ufgreber@zool.unizh.ch

1. *Abbreviations used in this paper:* Ad, adenovirus; Ad2, adenovirus type 2; Dyn, p50/dynamitin; ES, elementary speed; FISH, fluorescence in situ hybridization; GFP, enhanced green fluorescent protein; MAP, microtubule-associated protein; MT, microtubule; MTB, microtubule-binding domain; MTOC, microtubule organizing center; pFA, paraformaldehyde; p.i., post infection; TC7/MAP4/MTB–GFP, TC7 cells stably expressing the hybrid of MAP4/MTB–GFP; TR, Texas red; ts, temperature-sensitive; wt, wild-type.

or Ad5), enter a new host cell by receptor-mediated endocytosis, reach the cytosol by acid-dependent disruption of the endosomal membrane, translocate to the nuclear envelope, disassemble the capsid at the nuclear pore complex, and import their genome into the nucleus (for reviews see Greber, 1998a,b). Ads have been detected in association with cellular MTs (Dales and Chardonnet, 1973; Miles et al., 1980), passing from nerve termini to cell bodies by axonal transport (Ghadge et al., 1995; Ridoux et al., 1994) and binding to isolated MTs in vitro (Luftig and Weihing, 1975; Weatherbee et al., 1977). It is, however, not known if MTs are required for directional transport of the virus to the nucleus.

The MT network of an interphase cell is a dynamic polarized structure. Relatively stable minus ends are localized to the MT organizing center (MTOC), which is typically located at a perinuclear position in cultured cells (Mandelkow and Mandelkow, 1995). The dynamic, fast-growing and fast-shrinking plus ends extend towards the cell periphery (Desai and Mitchison, 1997). Directional movement along MTs is mediated by motor proteins which hydrolyze ATP to induce conformational changes in their structure. Motor proteins are needed for a variety of cellular activities, such as positioning of the mitotic spindle apparatus, movement of mitotic chromosomes, vesicular trafficking and maintenance of cell shape (Vallee and Sheetz, 1996; Hoyt et al., 1997; Hirokawa et al., 1998). Motors are classified according to the sequences of their motor domains and the directionality of their motion (Vale and Fletterick, 1997; Hirokawa, 1998). Kinesin superfamily motors typically move towards the MT plus ends, whereas dynein motors mediate minus end–directed movements. Alternatively to moving along MT tracks, motor proteins can produce directional movement by promoting local MT depolymerization and holding onto the ends of the depolymerizing MTs (Waters and Salmon, 1996).

The vast majority of the MT-dependent minus end–directed transport processes in interphase cells require dynein, which is typically associated with dynactin. The mammalian dynein is composed of two heavy chains, which contain motor domains, and four intermediate chains and light intermediate chains (Vallee and Sheetz, 1996). Dynein is thought to be nonfunctional for minus end–directed cargo transport, unless associated with dynactin, a heterooligomeric complex of at least nine different polypeptides (Schroer, 1996; Holleran et al., 1998). This concept has been reinforced experimentally by overexpression of the dynactin component p50/dynamitin, which is thought to dissociate the dynactin complex and severely affects mitosis, and also vesicular trafficking and organelle distribution in interphase cells (Echeverri et al., 1996; Burkhardt et al., 1997; Ahmad et al., 1998).

Despite much progress on the molecular and cellular anatomy of MT motors and their interactions with membranous cargo, much less is known about the MT-dependent transport of membrane-free particles. Another unresolved question concerns the regulation of directionality of cargo movement. To develop an in vivo experimental system for directional motility of a membraneless cargo, we decided to study the dynamics of Ad2 particles in living cells, knowing that the entry process of this virus is directed to the cell nucleus with exceptionally high efficiencies (Greber et al., 1993). Our results in HeLa and TC7 cells show that movement of cytosolic Ad2 towards the nucleus depends on intact but not dynamic MTs. Time-lapse fluorescence microscopy indicated that cytosolic wild-type (wt) and also endosomal mutant viruses moved with micrometer per second velocities in quasi-straight directions over several micrometers, either towards the MTOC or to the periphery. When the MT network was depolymerized with nocodazole, such long-range transport was abolished and virus distributed randomly in the cytoplasm. DNA import into the nucleus was effectively inhibited under these conditions, implying that intact MTs are instrumental for a successful infection. Immediately after restoring MTs, switching between plus- and minus end–directed virus motilities was observed at 0.5–1 Hz frequencies, either in the cell periphery or near the MTOC, suggesting that single virus particles engaged with both plus- and minus end–directed motors. Overexpression of p50/dynamitin significantly reduced the extent and the frequency of minus end migration of cytosolic Ad, and, surprisingly, increased the frequency, but not the extent of plus end–directed motility. In these cells, the population speed was clearly directed to the periphery, unlike in control cells, which transported wt Ad2 towards the MTOC. Dynamitin overexpression, like the depolymerization of MTs with nocodazole, did not affect the ability of wt virus to release a fluid-phase marker from endosomes suggesting that virus escape from endosomes neither required MTs nor dynein/dynactin. Together, the data illustrate that cytosolic Ad uses both minus- and plus end–directed MT-dependent motors at micrometer per second velocities, yet, it crosses the cytoplasm at population speeds of micrometers per minute.

This study is, together with two recent reports on electron-dense materials underneath the flagellar membrane (Cole et al., 1998; Pazour et al., 1998), one of the few examples describing fast bidirectional MT-dependent motilities of a nonmembrane bonded particle. Our results extend on the notion that directional MT-dependent transport is not only needed to establish and maintain an asymmetric distribution of cell organelles, but also functions to direct incoming virus particles to the site of replication.

Materials and Methods

Cells, Viruses, Antibodies, and Chemicals

HeLa cells (human cervical epitheloid carcinoma) were grown as described earlier (Greber et al., 1997). TC7 cells (African green monkey kidney) and the TC7 clone TC7/MAP4/MTB–GFP stably transfected with a cDNA encoding the MT-binding domain of the MT-associated protein 4 (MAP4) linked to enhanced green fluorescent protein (eGFP) were kindly provided by J. Bulinski (Columbia University, New York, NY) (Nguyen et al., 1997). Wt Ad2 and temperature-sensitive (ts)1 mutant Ad2 were grown and isolated as described (Greber et al., 1996). Labeling with Texas red (TR) was exactly as published (Greber et al., 1998). γ-Tubulin was visualized in 3% pFA-fixed (20 min at room temperature) and methanol-extracted (5 min at −20°C) HeLa cells using the mouse monoclonal antibody TU-30 (obtained from P. Draber, [Institute of Molecular Genetics, Prague, Czech Republic]) (Novakova et al., 1996). Mouse monoclonal anti-tyrosinated α-tubulin antibody (mAb 1A2) was obtained from T. Kreis (University of Geneva, Geneva, Switzerland) (Kreis, 1987).

Anti–β-tubulin antibody (N357; Amersham) was used on methanol-fixed cells. Rabbit anti-nuclear lamins A, -B, and -C peptide antibody 8188 was supplied by L. Gerace (Scripps Research Institute, La Jolla, CA) and used as described (Greber et al., 1997). Mouse monoclonal anti-Polyoma virus middle T tag was obtained from J.C. Perriard (Eidgenössische Technische Hochschule, Zürich, Switzerland) (Grussenmeyer et al., 1985; Komiyama et al., 1996). Nocodazole was purchased from Sigma, taxol from Calbiochem-Novabiochem, and fluorescent dyes from Molecular Probes. Drugs were dissolved as 1,000× stocks in DMSO and used as indicated. No drug treatment included appropriately diluted DMSO.

Time-lapse Fluorescence Microscopy

HeLa cells, TC7, or TC7/MAP4/MTB–GFP cells (Nguyen et al., 1997) were grown on glass coverslips (Assistent, Winigor) in DME-10% FBS medium to ~20–50% confluency. Geneticin (100 μg/ml; Alexis Biochemicals) was included to maintain the TC7/MAP4/MTB–GFP cells. TR-labeled virus (1–2 μg/ml) was added in warm RPMI-0.2% BSA-20 mM Hepes medium, pH 7.4, for 5 min. Cells were washed several times in RPMI medium. The coverslip was mounted to a homemade temperature-regulated chamber, covered with a glass slide, sealed with silicon grease, and then perfused with warm RPMI medium using a plastic syringe. The system was mounted to an electronically controlled inverted fluorescence microscope (model DM IRBE B; Leica) equipped with a Leica 100× oil immersion objective (NA 1.3), a differential interference contrast (DIC) polarizer and fluorescein (490/7.3 nm), TR (600/10.1 nm), and Cy5 (649/11.4 nm) excitation filters with bandpass emission filter cubes of 510/20 nm (Dichroic 495), 615/30 nm (Dichroic 595) and 690/40 nm (Dichroic 660), respectively (Omega Optical). Fluorescence images were recorded with a digital, back-illuminated charge coupled device camera (TE/CCD-1000, TKB grade 1; Princeton Instruments) onto a 1,000 × 800 pixel chip (15 × 15 μm/pixel) at 12 bit/500 kHz/−40°C using a PCI interface card and the MetaMorph software package (Universal Imaging). Exposure times in the TR channel were between 0.2 and 0.4 s, yielding less than 1% saturation of individual pixels. Intervals between subsequent exposures were between 1.2 and 2.6 s depending on the size of the region of interest selected in a given experiment. Observations typically lasted 1–3 min and were made between 20 and 40 min postinternalization, unless otherwise indicated. At the beginning or end of the experiment, the GFP fluorescence and/or DIC was recorded to visualize either the MT network (MAP4/MTB–GFP) or GFP alone to identify transfected cells. Individual virus particles showing linear translocations were tracked and velocities (distance between subsequent frames per time interval) determined using the MetaMorph tracking module. Velocities <0.1 μm/s were within the experimental error of our setup. The uncertainty in the tracing analysis was ±1 pixel (15 μm at 100× magnification) yielding a mean error of 1.45 pixels/time interval.

Statistical Analysis

Elementary speeds (ES, elementary motion steps per time interval) were determined for motile TR-labeled particles by recording x,y coordinates as described above. Motile particles were operationally defined as those particles that could be unequivocally traced in at least 20 subsequent frames and translocated in more than five subsequent frames over at least 0.5 μm in either plus or minus end direction. Depending on the cell type and the length of the observation period, 20–80% of the particles showed continuous plus- or minus end–directed translocation in five or more subsequent frames over several micrometers. Plus end–directed motility was defined as $d_i - d_{i+1} < 0$ and minus end–directed motility as $d_i - d_{i+1} > 0$, (d_i is the particle distance from the presumptive MTOC in frame i, and d_{i+1} the distance from the MTOC in frame i+1). Calculated ES < 0.1 μm/s were counted as no motility events. An apparent net population velocity was determined by the difference between all minus- and plus end–directed distances divided by the total sampling time. A one-sided *t* test was applied at the 95% confidence level to compare the MTOC- and the periphery-directed mean population speeds of wt and ts1 virus in a given cell type under different conditions. Frequencies of MTOC- and periphery-directed speeds and no movements were compared in a chi square test and evaluated at 95% confidence level.

Indirect Immunofluorescence and Laser Scanning Confocal Microscopy

Cells were grown on 12-mm glass coverslips in DME-7% FBS, transferred to cold RPMI medium containing 0.2% BSA, buffered with Hepes-NaOH to pH 7.4 (binding medium) and incubated with TR-labeled Ad2 (0.2–0.5 μg per 0.2 ml) for 90 min, followed by an incubation in warm DME-BSA at 37°C for indicated times as described (Greber et al., 1997). Samples were fixed in pFA, mounted in paraphenylene diamine (0.5%)-glycerol (80%)-Tris (20 mM), pH 8.8, and analyzed for single or double epifluorescence on a Reichert-Jung Polyvar microscope (Merck) equipped with Nomarski DIC, a fluorescein filter set (485/10, BP 540/20), and a TR filter set (557.5/27.5, LP 615) linked to an eight-bit CCD video camera (model C5405; Hamamatsu Photonics). Images were collected with the Argus-20 imaging acquisition software (Hamamatsu Photonics) and batch-processed with Adobe Photoshop (Adobe Systems) on an Apple Macintosh computer (Quadra 650). Triple fluorescence experiments were analyzed on a Leica DM IRBE inverted microscope equipped with a 63× lens and FITC, TR, and Cy5 filter sets as specified above. Confocal microscopy was conducted on a Leica DM IRBE inverted microscope equipped with a 100× lens and a Leica TCS 4D confocal laser scanning device (Elektronenmikroskopisches Zentrallabor of the University of Zürich, also see Greber et al., 1997). Typical section thickness was estimated to be 300–400 nm based on the pinhole settings.

Plasmids and DNA Experiments

GFP-encoding plasmid DNA (gift of S. Zimmermann; Invitrogen, Zürich, Switzerland) was transfected into TC7 or HeLa cells alone or together with dynamitin-encoding DNA (gift of R. Vallee, University of Massachusetts, Worcester, MA) (Echeverri et al., 1996) at a molar ratio of 2:1 using Lipofectamine™ (5 μl/μg DNA; GIBCO BRL) or TransFast™ (7 μl/μg DNA; Promega). Under these conditions more than 90% of the transfected cells expressed both GFP and dynamitin at 24 h posttransfection. In situ hybridizations to detect incoming viral DNA were carried out as described (Greber et al., 1997), except that the 42° and 60°C wash steps were omitted. A control plasmid encoding hexon loop 1 (amino acids 160–336) was constructed by PCR using the synthetic oligonucleotide AGCTACAAGCTTGGATCCCATATGGAAGAGCAAAACGCTCGAGAT as an NH_2-terminal primer and CTCGATGCTGAGCCCCGGGTTATTCCATTGGCATGTATTCTCGGGTCTGTTTGGCATAGATTG as a COOH-terminal primer, respectively. The latter also encoded the polyoma middle T tag (EEYMPME, single amino acid letter code) in front of the multiple cloning site. PCR products were ligated into the polylinker of pSCT2+ using the HindIII and SmaI restriction sites (Auerbach et al., 1997) and amplified in *Escherichia coli*. The loop 1 insert of the clone used here was confirmed by dideoxy sequencing.

Electron Microscopy and HRP Detection

Alcian blue–coated glass coverslips were prepared as follows. Glass coverslips (12 mm; Assistent) were washed in a glass beaker with 1 N HCl for 10 min and rinsed with distilled water, 90% methanol, 50% methanol, and then again with distilled water. Alcian blue (1% wt/vol Alcian blue-tetrakis[methyl-pyridinium]chloride in water [Sigma]) was added and the liquid brought to boiling for 30 s in a microwave oven. Coverslips were rinsed several times in water, placed between filter paper and sterilized by autoclaving and drying. HeLa or TC7/MAP4/MTB-GFP cells were seeded onto glass coverslips coated with Alcian blue. Wt Ad2 (50 μg/ml) was bound to the cell surface in the cold for 90 min and internalized at 37°C in the presence of HRP (20 mg/ml, Type II, 150–200 U/mg; Sigma) in DME containing 0.2% BSA for 15 min. HRP was washed out with warm DME containing 0.2% BSA and cells were further incubated at 37°C for 15 min. Samples were quickly washed in PBS several times and fixed in PBS containing 2% glutaraldehyde (Electron Microscopy Sciences, Merck) for 30 min at room temperature, washed in PBS, and then stained for HRP activity in 0.1 M Tris-HCl, pH 7.4, 1 mM $MgCl_2$ containing 0.5 mg/ml diaminobenzidine (Sigma) and 0.03% hydrogen peroxide (Fluka). Samples were then processed for Epon embedding and analyzed by EM as described (Greber et al., 1997).

Results

We have generated two types of fluorescent adenoviruses, wt and an endosomal mutant virus, ts1, to visualize virus trafficking between the cell periphery and the nucleus in vivo and to determine the mechanism of cytoplasmic mo-

tility, which allows virus targeting to the nuclear membrane.

Physiological Temperature Is Needed for Nuclear Targeting of Ad2

The structural organization of the cytoplasm typically restricts the diffusional mobility of artificial particles of 50 nm in diameter to a few square micrometers per second (Luby-Phelps, 1994; Seksek et al., 1997). Particles larger than 50 nm, such as Ad2, are expected to have essentially no diffusion mobility under physiological conditions. To test if cytosolic virus was localized to the nucleus in the absence of energy metabolism at a reduced temperature, we bound TR-labeled Ad2 to the surface of HeLa cells in the cold and internalized for 29 min at 37°C. During this time virus is taken up into the cytoplasm but is not yet targeted to the nucleus (Greber et al., 1993, 1997). Cells were subsequently shifted to 4°C and incubated in the cold for up to 60 min postinternalization, whereas control cells were kept at 37°C. Since exposure of cells to reduced temperatures causes depolymerization of MTs, targeting was also analyzed in cells that had been pretreated with the MT-stabilizing drug taxol. In control cells the large majority of virus particles was directed to the nucleus during the 60-min internalization, in agreement with previous results (Fig. 1) (Greber et al., 1997). In contrast, at reduced temperatures, with or without taxol treatment, virus particles were found randomly distributed in the cytoplasm at 60 min. The same result was obtained if the cold incubation was extended up to 90 min (data not shown). Virus particles also remained cytoplasmic if cellular ATP levels were reduced after 30 min of internalization by shifting cells into a glucose-free medium containing 10 mM sodium azide and 20 mM 2-deoxy-D-glucose (data not shown). These results confirmed that incoming Ad2 does not move through the cytoplasm by diffusion, but uses some form of mediated transport.

Microtubule-dependent Minus End–directed Transport of Cytosolic Virus

Previous EM studies have detected Ads in close association with MTs both in vivo and in vitro (data not shown) (Dales and Chardonnet, 1973; Luftig and Weihing, 1975; Weatherbee et al., 1977; Miles et al., 1980). To ask whether MTs are actually needed for directional transport of virus to the nucleus, we first tested if virus could be detected at the MTOC in cultured epitheloid HeLa cells. In these cells the MTOC predominantly contains the minus ends of MTs and is located in the perinuclear area as confirmed with an anti–γ-tubulin immunostaining and confocal microscopy (Fig. 2 A). As expected (i.e., Moudjou et al., 1996), γ-tubulin was found all over the cytoplasm but was concentrated at a perinuclear location (Fig. 2 A, green dot). Of a total of 101 examined cells, 75% had a perinuclear enrichment of incoming virus at 60 min postinfection (p.i.). At 15 min postinternalization no enrichment was observed.

We next analyzed if intact MTs were required for virus targeting to the nucleus. HeLa cells were incubated with 20 μM nocodazole for 30 min and virus was bound to the cell surface for 60 min in the cold to synchronize infection and to further depolymerize MTs. Cells were then shifted to 37°C in drug-containing medium for 75 min. Under these conditions, MTs were completely depolymerized as shown with mAb 1A2 and anti–β-tubulin immunostainings (data not shown). Nocodazole strongly, but not completely inhibited localization of TR-labeled virus to the nuclear envelope as indicated by confocal microscopy (Fig. 2 B, panel c). Similar results were obtained if the internalization time was extended to 135 min (data not

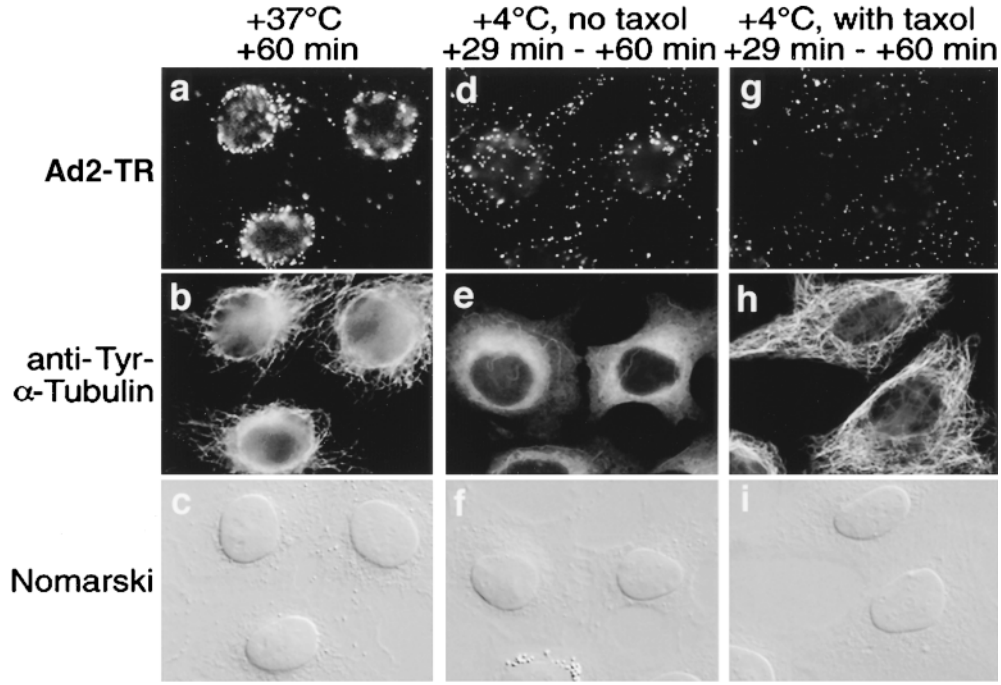

Figure 1. Ad2 targeting to the nucleus requires physiological temperature. TR-labeled Ad2 was cold bound to HeLa cells in the absence (a–f) or presence of taxol (25 nM) including a 15-min preincubation with drug in growth medium at 37°C (g–i). Cells were warmed for 29 min (d–i) followed by a cold incubation up to 31 min in the absence (d–f) or presence (g–i) of taxol or were warmed for 60 min in the absence of drug (a–c). Samples were fixed with pFA and analyzed by epifluorescence microscopy.

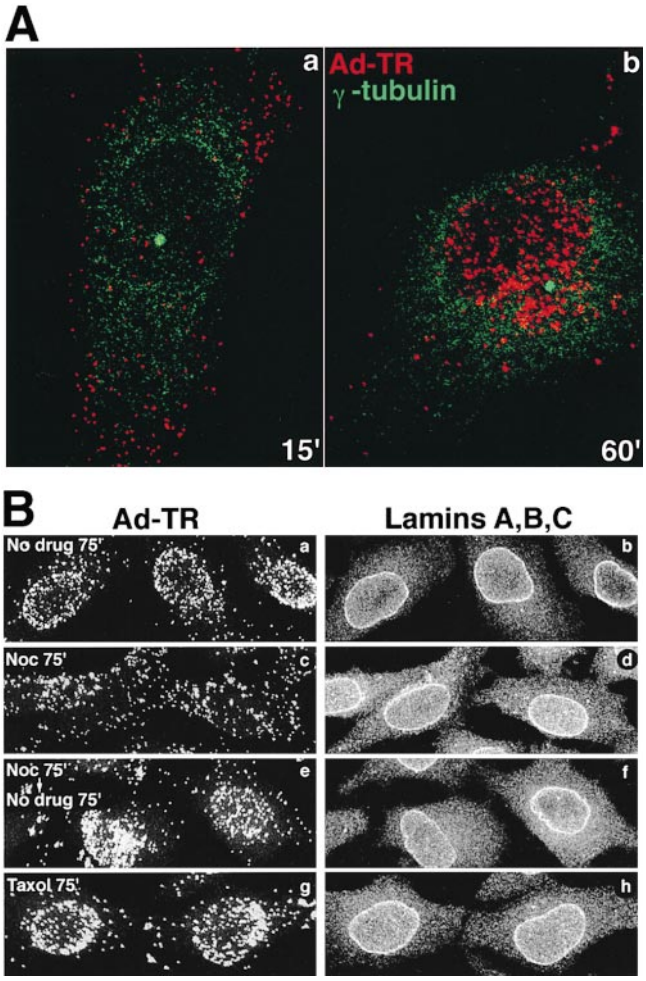

Figure 2. Microtubule-dependent transport of Ad2 to the MTOC/nuclear envelope. (A) TR-labeled Ad2 was bound to HeLa cells in the cold and internalized for 15 (panel a) or 60 min (panel b). Cells were labeled for γ-tubulin and analyzed by confocal laser scanning microscopy (shown are the sections that contained the perinuclear punctate γ-tubulin signal only). Virus particles (red) and γ-tubulin (green) are pseudocolored. (B) TR-labeled Ad2 was bound to HeLa cells in the cold in the absence (panels a and b) or presence of either 20 μM nocodazole (panels c–f) or 25 nM taxol (panels g and h). Drug treatment included a 30-min preincubation with drugs before virus binding. Cells were warmed to 37°C in the presence or absence of drugs for 75 min (panels a–d, and h) or treated with nocodazole for the same time followed by an incubation without drug for 75 min (panels e and f). Cells were fixed in pFA and stained for lamins A, -B, and -C using anti-rabbit FITC and analyzed by confocal microscopy for TR and FITC fluorescence. Complete stacks of optical sections are shown.

shown), thus suggesting that the low level of nuclear targeting was most likely due to particles entering from a plasma membrane area near the nucleus. If MTs were restored by washing out nocodazole for 75 min, significant virus targeting to the nucleus was observed, similar to cells not treated with the drug (Fig. 2 B, panels a and e). These results were confirmed by analyzing viral DNA import into the nucleus in nocodazole-treated cells using fluorescence in situ hybridization (FISH) and confocal laser scanning microscopy at 180 min p.i. Control cells (no drug) had a strong signal of viral DNA inside the nucleus as concluded from an anti-lamin immunostaining of the nuclear envelope (Fig. 3 a). Noninfected cells had no viral DNA signal, indicating that the FISH conditions were specifically detecting viral genomes (Fig. 3 c) (see also Greber et al., 1997). In nocodazole-treated cells most of the DNA signal was present in the cytoplasm, sometimes in an aggregated form (Fig. 3 d). Note that the combined cytoplasmic signal was somewhat lower than the nuclear signal in the control (no drug)-treated cells, partly because some cytoplasmic virus had been artificially released during the FISH treatments. The absence of viral DNA in the nucleus was not due to a lack of detection or rapid nuclear export, since viral genomes were readily found in the nucleus of cells that were treated with nocodazole beginning at 90 min p.i., when the majority of virus particles had already arrived at the nuclear envelope (Fig. 3 f). The cytoplasmic DNA signals in the nocodazole-treated cells decreased after washing out the drug and a strong nuclear DNA signal appeared (Fig. 3 e). Taken together, these results suggested that intact MTs are needed for targeting of incoming virus particles to and for import of viral DNA into the nucleus.

It was possible that nocodazole affected endocytosis and/or virus escape from the endosome. We therefore measured the internalization of [^{35}S]methionine virus into drug-treated cells using a cell surface trypsinization assay, which measures virus uptake by the emergence of a trypsin-resistant form of the major capsid protein hexon (Greber et al., 1993). The results indicate that in the presence of nocodazole half of the virus particles were endocytosed at 15 min postwarming, whereas in control cells the half-time of internalization was ~9 min (Fig. 4 A). The efficiency of entry at 30 min postwarming was close to 75% under both conditions. The remaining viruses were most likely shed from the cells into the medium (Greber et al., 1993). The data demonstrated that virus uptake into cells lacking intact MTs was slightly slower, but no less efficient than into control cells, in agreement with earlier observations showing that nocodazole had no effect on the formation of endocytic vesicles (Gruenberg et al., 1989).

We next asked if virus was able to escape from endosomes in cells lacking MTs. To visualize both endosomes and virus particles at high resolution we used a fluid-phase endosomal marker, HRP, in combination with EM (Fig. 4 B). HeLa cells were pretreated with nocodazole for 15 min. Wt or a mutant virus, ts1, which is unable to escape from endosomes (Greber et al., 1996), were bound to the cells at 4°C. Ts1 has a point mutation P137L in the protease reading frame and, when grown at the nonpermissive temperature, produces particles, which fail to escape from endosomes in a new round of infection (Weber, 1995; Greber, 1998b). Virus internalization then occurred in the presence of HRP and drug for 15 min at 37°C, followed by a 15-min chase without HRP in the presence of nocodazole. HRP activity was visualized by incubating the fixed cells with diaminobenzidine, which is converted to an electron dense product by HRP (Doxsey et al., 1985). Control cells (no drug) contained numerous cytosolic wt particles, also near nuclear pore complexes, but only few viruses were detected within vesicular structures (Fig. 4 B, panel

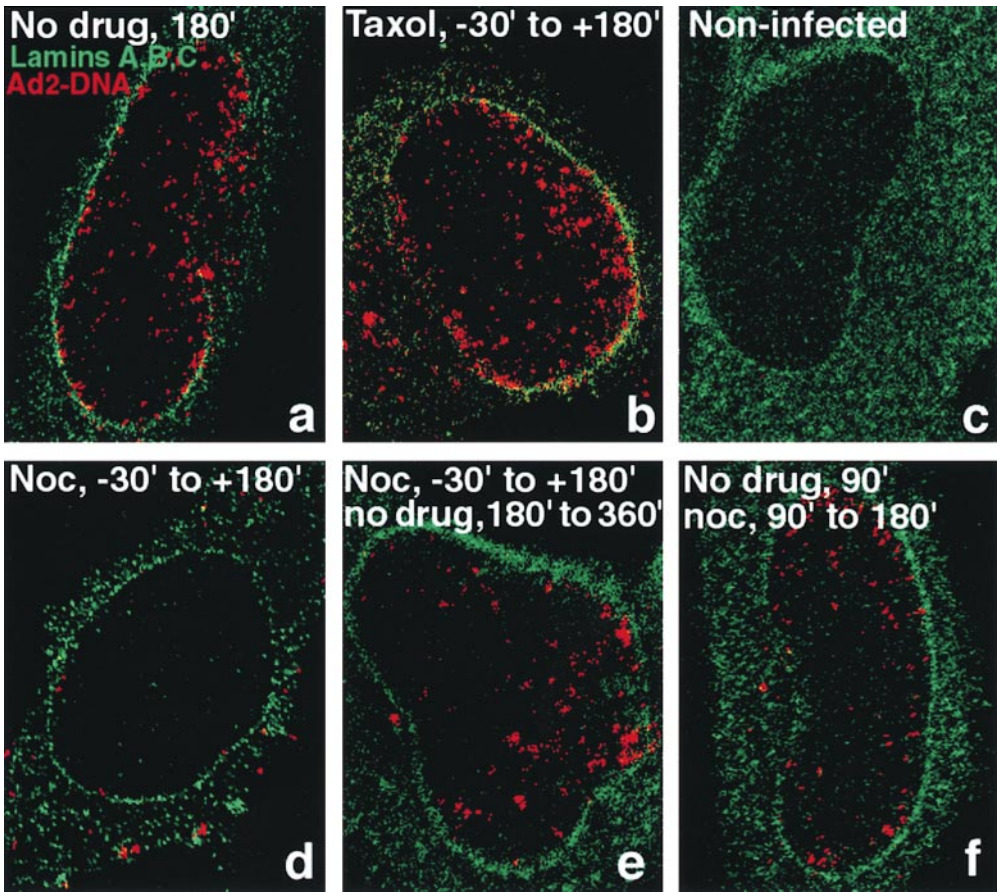

Figure 3. Inhibition of Ad2 DNA import in nocodazole-, but not taxol-treated HeLa cells. HeLa cells were pretreated with either nocodazole (20 μM) or taxol (25 nM) as described in Fig. 2. Wt Ad2 (20 μg/ml) was bound in the cold in the presence or absence of drugs and internalized in DME-BSA medium in the absence (a) or presence of taxol (b) or nocodazole (d) for 180 min. A parallel sample of nocodazole-treated cells was washed several times in drug-free medium and incubated for an additional 180 min in DME-BSA (e). Alternatively, nocodazole was added to cells from 90 up to 180 min p.i. (f). All samples including noninfected cells (c) were then analyzed by in situ hybridization using TR-labeled genomic Ad2 DNA followed by antilamin immunolabeling of nuclear envelopes and confocal laser scanning microscopy.

a). Interestingly, these cells contained essentially no vesicles with HRP reaction product, in contrast to noninfected cells, suggesting that contents of endocytic vesicles were released (Fig. 4 B, panels a and b) (Prchla et al., 1995). Nocodazole-treated cells contained numerous virus particles in the cytosol and only few HRP-positive endosomes, similar to control cells (Fig. 4 B, panel b). These cytosolic particles were clearly distinguishable entities and often occurred in clusters. Ts1 viruses, on the other hand, were exclusively detected within HRP-containing vesicles, as expected (Fig. 4 B, panel c) (Greber et al., 1996). We concluded that MTs were not needed for Ad2 uptake into cells and delivery to the cytosol, but were required for targeting of cytosolic virus to the nucleus.

Microtubule-dependent Transport of Cytosolic and Endosomal Viruses at Micrometers Per Second

A recent report stated that fluorophore-labeled Ad5 particles were able to move in the periphery of human A549 cells over short distances with apparent velocities of 0.5–0.6 μm/s (Leopold et al., 1998). We aimed at analyzing the mechanisms underlying this motility and wanted to test a possible involvement of MTs.

We conducted extensive particle tracking analysis in TC7 cells (an African green monkey kidney cell line) and in HeLa cells. The TC7 cells have a particularly large and flat cytoplasm and are well suited for studies of cytoplasmic movement of Ad since they efficiently internalize and target virus to the nucleus (data not shown). To determine the approximate position of the MTOC we used in some experiments a TC7 clone, which was stably transfected with a cDNA encoding a GFP hybrid of the MAP4 MT-binding domain (MAP4/MTB–GFP; Bulinski et al., 1997; Nguyen et al., 1997). This cell line was viable in our hands for more than 20 passages (Olson et al., 1995). TR-labeled Ad2 was internalized at 37°C for 30 min and the coverslip was mounted to a temperature-controlled heating chamber placed on an inverted fluorescence microscope. Fluorescence images were recorded in the TR channel at 1.2–2.6-s frame intervals over several min as described in Materials and Methods. We use the term ES to define directional movement of particles between two subsequent frames, negative ES indicating movement to the MTOC (minus end) and positive ES to the periphery (plus end). At the end of the recordings the MAP4/MTB–GFP fluorescence was captured. A representative experiment is shown in Fig. 5 where we traced three different particles. One peripheral particle (arrow) was followed throughout the experiment and two MTOC-neighboring particles were traced at the end of the experiment in frames 92–98 (Fig. 5 B, arrowheads). The peripheral particle moved ~30 μm in a quasi-straight direction towards the MTOC. In Fig. 5, C and D we plotted the distances of the particle from the MTOC and the ES for each frame. The ES defined two distinct types of activity periods. The first type of activity

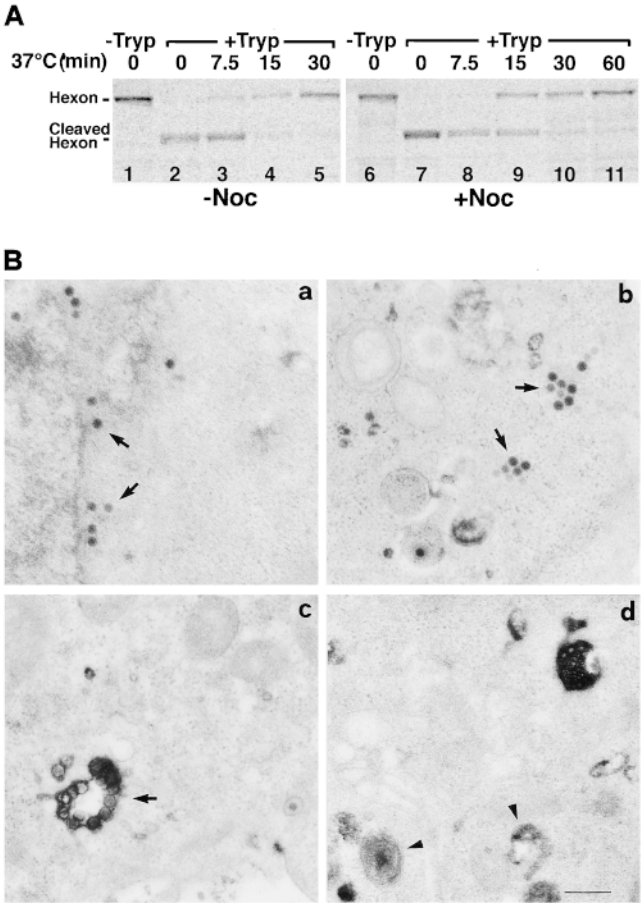

Figure 4. Ad2 arrives in the cytosol in the absence of intact microtubules. (A) HeLa cells were either kept in drug-free medium (lanes 1–5) or pretreated with 20 μM nocodazole at 37°C for 15 min (lanes 6–11). [^{35}S]methionine Ad2 was bound in the cold, followed by warming in the presence or absence of nocodazole for indicated times. Surface-bound virus was digested with trypsin for 1 h in the cold followed by analysis of cleaved and trypsin-resistant hexon by SDS-PAGE and phosphorimaging as described earlier (Greber et al., 1993). (B) HeLa cells were either treated with 20 μM nocodazole (panel b) or left in drug-free medium (panels a, c, and d) as described in A. 50 μg/ml wt Ad2 (panels a and b) or 50 μg/ml ts1 virus (panel c) or no virus (panel d) was bound at 4°C for 90 min. Cells were warmed to 37°C in growth medium containing 20 mg/ml HRP with or without nocodazole for 15 min and then incubated in HRP-free medium for 15 min, fixed, and then prepared for thin section EM. HRP activity was visualized using diaminobenzidine. Bar, 0.5 μm.

occurred between frames 39–44 and 68–79 and contained exclusively MTOC-directed motions. This activity resulted in efficient particle advancement towards the MTOC and typically lasted for several seconds reaching elementary speeds of 0.17–2.63 μm/s. The other type of activity was characterized by rapidly alternating minus- and plus end–directed ES up to 0.5 μm/s at nearly equal extents and frequencies (Fig. 5, frames 1–38, 45–67, and 80–104). Such activities resulted either in a net minus end–directed speed of 2–4 μm/min (frames 44–68), or yielded no net movement (frames 1–38 and 80–104). Note that from frames 80–104, two additional MTOC-near particles still showed net minus- (Fig. 5 B, solid arrowhead) and plus end–directed (Fig. 5 B, open arrowhead) movements, indicating that cells and viruses were still motion competent.

A population analysis of 958 ES from 15 different particles in TC7/MAP4/MTB–GFP cells and 729 ES from 19 different particles in the parental TC7 cells indicated a tailed distribution of both the MTOC- and the periphery-directed speeds, with maximal ES occurrence between 0.1 and 0.2 μm/s (Fig. 5, E and F) (Table I). In MAP4/MTB–GFP cells, all the MTOC-directed speeds were more prominent than the periphery-directed speeds, in contrast to the parental TC7 cells, in which less minus- and more plus end–directed ES occurred. However, even in these cells, the minus end–directed motion was dominant over the plus end–directed motion as indicated by the mean population speed of −0.06 μm/s. The MAP4/MTB–GFP-expressing cells contained significantly more active particles than the parental TC7 or HeLa cells. The number of immobile particles (ES smaller than 0.1 μm/s) amounted to 12.8, 28.4, and 41.4% for TC7/MAP4/MTB–GFP, parental TC7 and HeLa cells, respectively (Tables I and II). The mean minus end–directed speed was 0.50 μm/s in both TC7 cell types, but the mean and also the peak plus end–directed speeds were significantly smaller in the MAP4/MTB–GFP expressing cells than in the parental cells (Tables I and II). Accordingly, the population mean speed (comprising all the traced particles) was significantly shifted to the MTOC direction in the TC7/MAP4/MTB–GFP cells (−0.21 μm/s) compared with TC7 cells (−0.06 μm/s) or HeLa cells (−0.03 μm/s). Although the mean minus- and plus end–directed speeds in HeLa cells were significantly smaller than in TC7 cells (perhaps relating to the fact that the TC7 cells allowed longer tracking analysis than the HeLa cells), the calculated population average speeds for wt virus were in good agreement with the observed enrichment of virus near the MTOC starting at ~25 min to 40 min p.i. This reflects the half-time of virus penetration of endosomes which is ~15 min (Greber et al., 1993).

To confirm that the above measured speeds were truly derived from cytosolic viruses, we analyzed the trafficking of an endosomal mutant Ad2, ts1, in TC7/MAP4/MTB–GFP cells and in parental TC7 cells. Unlike wt virus, ts1 had a population mean speed of −0.02 μm/s in TC7/MAP4/MTB–GFP cells and +0.04 μm/s in TC7 cells indicating slow minus- and plus end–directed net movements (Table I). Accordingly, we have not observed ts1 virus accumulation near the MTOC up to 60 min p.i. Like wt virus, ts1 showed a tailed distribution of ES, with the majority in the range of 0.1–0.2 μm/s (Fig. 6 E). In both cell types, about 22.5% of the ES were less than 0.1 μm/s. A typical ts1 trace in a MAP4 overexpressing cell shows how a virus particle moved from a location proximal to the MTOC towards the periphery with ES of up to 1.7 μm/s and from there returned to an MTOC-near location with ES of up to 2.3 μm/s (Fig. 6). Taken together, the data illustrate a distinct dynamic behavior of wt and endosomal viruses further supporting the notion that wt Ad2 travels as a naked particle along MTs.

Switching between Minus- and Plus End–directed Motions

The observation that periods of minus end–directed Ad2

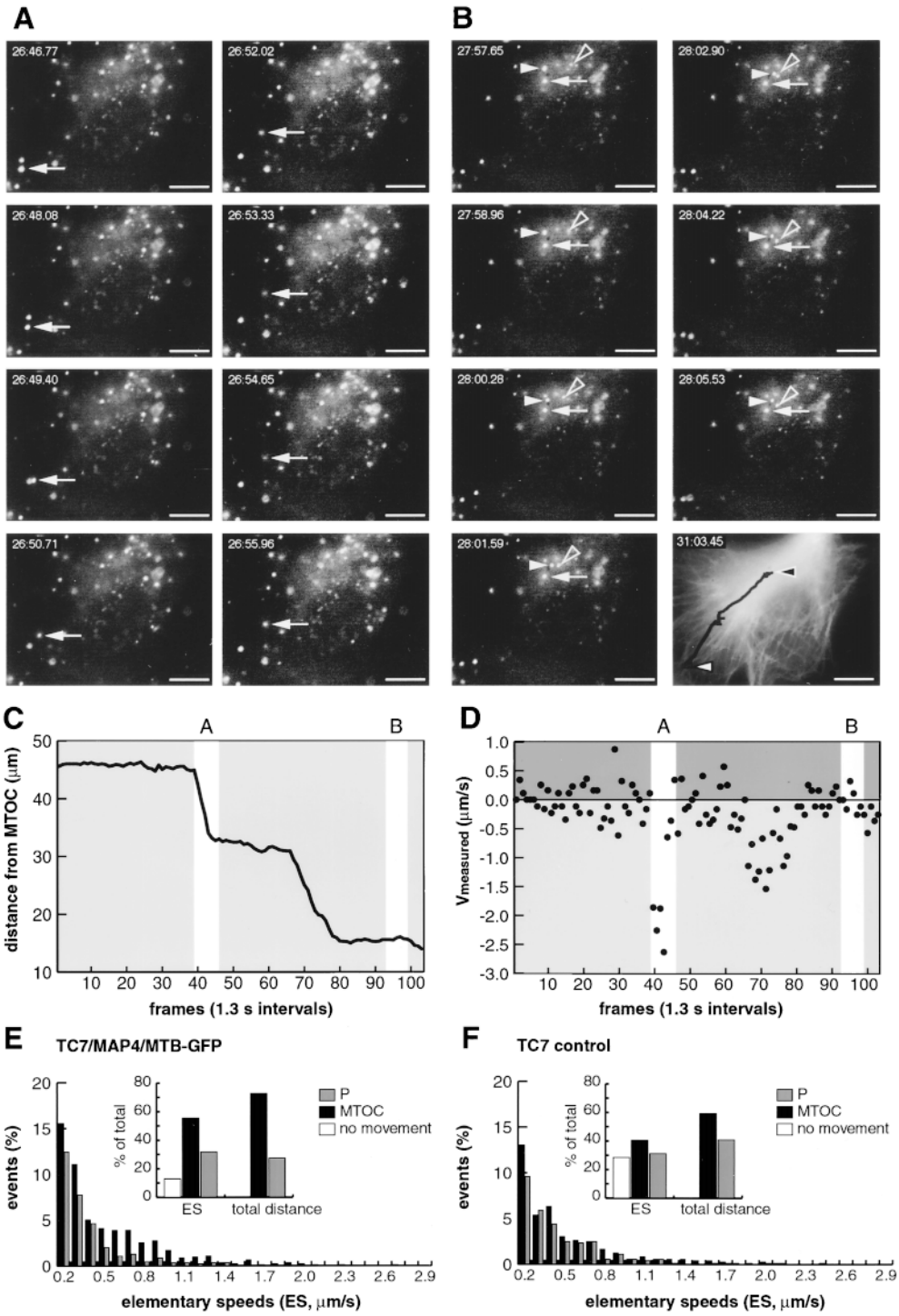

Figure 5. Fast minus end–directed transport dominates over plus end–directed transport of wt Ad2: analysis in TC7/MAP4/MTB–GFP cells (A–E) and TC7 parental cells (F). (A and B) Images of TR-Ad2 were recorded with intervals of 1.3 s starting 30 min p.i. (time stamp displaying minutes: seconds.centiseconds). One particular virus particle (arrow) was followed in 104 subsequent frames. Frames 39–46 and 93–99 (with two additional active particles) are shown in A and B, respectively. (C) The distance of the traced particle (A and B, arrows) to the presumptive MTOC was plotted at each frame, thus highlighting periods of activity and relative immobility. (D) ES of the traced particle were calculated between subsequent frames and plotted as micrometers per second indicating minus end–directed movement as negative and plus end–directed movement as positive speeds. (E) Population analysis of motile particles (see Materials and Methods). 958 ES from 19 different virus particles and six different cells (see also Table I) were measured, grouped into 0.1-μm/s intervals, and then plotted as either minus- (dark bars) or plus end–directed (grey bars) events. ES < 0.1 μm/s were within the experimental error and plotted as 0 (inset, open bar). Inset, cumulative representation of the minus- (dark bar) and plus end–directed ES (grey bar, 100% = 958) and distances (100% = 532.9 μm). For the distance calculations, only ES > 0.1 μm/s were included. (F) Population analysis of ES in parental TC7 cells not expressing MAP4–GFP with inset as in E (100% ES = 729, 100% distance = 495.6 μm). The corresponding movie is available at http://www.unizh.ch/~cellbio/jcb1999-1.html Bar, 10 μm.

transport were often followed by plus end–directed motions along an apparently linear track could in principle be explained by the dynamic instability of MTs (Waters and Salmon, 1996; Desai and Mitchison, 1997). In fact, growing and shrinking MTs were readily observed in TC7/MAP4/MTB–GFP cells, preferentially in the cell periphery (data not shown).

Dynamic turnover of MTs can be experimentally eliminated by incubating cells in low concentrations of taxol or nocodazole (Liao et al., 1995; Waterman-Storer and Salmon, 1997). To first test if dynamic MTs were needed for nuclear targeting of Ad2 we pretreated HeLa cells with 25 nM taxol for 30 min. Such treatment was sufficient to stabilize MTs against cold-induced depolymerization (Fig.

Table I. Frequencies and Extents of MTOC- and Periphery-directed ES and No Movement Frequencies (0) of Wt and Ts1 Ad2 in TC7, TC7/MAP4/MTB–GFP, and HeLa Cells

	MTOC			Periphery			0	Total			
	Peak	Mean	ES	Peak	Mean	ES	ES	Mean	ES	Particles	Cells
	μm/s	*μm/s*		*μm/s*	*μm/s*			*μm/s*			
TC7 Contr											
No drug	2.06	0.50 ± 0.34	295 (40.5%)	2.33	0.42 ± 0.23	227 (31.1%)	207 (28.4%)	−0.06 ± 0.22	729	15	8
TC7/MAP4-G											
No drug	2.63	0.50 ± 0.15	531 (55.4%)	1.38	0.31 ± 0.11	304 (31.7%)	123 (12.8%)	−0.21 ± 0.19	958	19	6
Tax	2.12	0.44 ± 0.19	340 (35.4%)	1.08	0.33 ± 0.23	228 (23.8%)	392 (40.8%)	−0.14 ± 0.15	960	18	7
Surface	0.19	0.12 ± 0.02	76 (8.3%)	0.20	0.11 ± 0.01	71 (7.8%)	769 (84.0%)	−0.00 ± 0.00	916	12	5
HeLa											
No drug	2.08	0.31 ± 0.14	555 (33.1%)	2.19	0.33 ± 0.15	427 (25.5%)	695 (41.4%)	−0.03 ± 0.17	1,677	28	11
DynGFP	2.13	0.22 ± 0.10	143 (17.7%)	1.08	0.30 ± 0.12	255 (31.5%)	412 (50.9%)	0.06 ± 0.10	810	25	9
GFP	1.36	0.36 ± 0.11	330 (37.3%)	1.45	0.34 ± 0.19	228 (25.8%)	327 (36.9%)	−0.05 ± 0.24	885	14	13
Noc	0.28	0.15 ± 0.02	65 (10.7%)	0.36	0.17 ± 0.05	82 (13.5%)	461 (75.8%)	0.04 ± 0.09	608	13	3
Surface	0.17	0.11 ± 0.01	24 (5.4%)	0.17	0.11 ± 0.02	24 (5.4%)	400 (89.3%)	0.00 ± 0.01	448	16	4
Ts1 Ad											
TC7 Contr											
No drug	2.48	0.36 ± 0.10	544 (35.5%)	2.12	0.39 ± 0.12	641 (41.9%)	346 (22.6%)	0.04 ± 0.08	1,531	15	7
TC7/MAP4-G											
No drug	2.28	0.33 ± 0.14	573 (40.6%)	1.84	0.30 ± 0.14	520 (36.9%)	317 (22.5%)	−0.02 ± 0.14	1,410	32	5
Tax	2.69	0.45 ± 0.19	422 (38.8%)	1.84	0.39 ± 0.23	369 (33.9%)	298 (27.4%)	−0.07 ± 0.18	1,089	19	3

Motilities of TR-labeled virus particles in control or drug-treated cells were recorded by time-lapse fluorescence microscopy using intervals between 1.2 and 2.6 s and analyzed as described in Materials and Methods. ES were calculated from the elementary motion steps of selected virus particles that were located well within the cell and were able to move in at least five subsequent frames over a minimal distance of 0.5 μm. ES were grouped according to their directionalities, MTOC (minus end), periphery (plus end), and no motility (0), and characterized in terms of peak speeds, mean speeds, and frequencies. The no motility category comprised movements of less than 0.1 μm/s, which was within the systematic error of our measurements. The total amounts of ES was between 448 and 1,677 and derived from three to seven independent experiments analyzing 13–32 different virus particles in 3–13 different cells, respectively. The mean plus- and minus end–directed speeds including the standard deviations were determined by averaging the corresponding mean velocities of individual particles. Total mean speeds (representing the population speeds) including the standard deviations were calculated for each particle that was traced. Minus values represent MTOC-directed speeds, positive values are periphery-directed speeds. (For significant differences between different mean speeds, see Table II.)

Movement frequencies were different in all cases listed above, except in the following instances (as analyzed in a chi square test). With wt Ad2: HeLa control versus HeLa GFP (peripheral, MTOC, and no motility); TC7 control versus TC7/MAP4/MTB–GFP (peripheral speeds); TC7/MAP4/MTB–GFP taxol versus HeLa control or HeLa GFP (peripheral and MTOC speeds). With ts1 Ad2: TC7/MAP4/MTB–GFP control versus TC7/MAP4/MTB–GFP taxol (periphery, MTOC).

1, e and h). Ad2-TR was bound to the surface and then internalized in the presence of the drug for 75 min. Similar to control cells, the majority of virus particles were localized to the nuclear envelope (Fig. 2, g and h). Viral DNA was readily detected inside the nucleus at 180 min p.i. using the FISH assay described above (Fig. 3 b). Likewise, treatment of TC7/MAP4/MTB–GFP cells with low concentrations of nocodazole (1–10 μM for 15 min) in the absence of cold incubations neither affected the MT network nor virus targeting to the nucleus (data not shown). We next analyzed Ad2 motility in MAP4/MTB–GFP-expressing TC7 cells in the presence of taxol or low nocodazole. As expected from the static entry analysis (Fig. 2 B), the population mean speeds towards the MTOC and the periphery were not significantly different from the control cells (Table I). In cells treated with low concentrations of nocodazole, we also observed peak minus- and plus end–directed speeds of up to 1.7 μm/s (data not shown). Although the frequencies of either minus- or plus end–directed motions were significantly decreased in the presence of taxol and the no movement frequencies were increased from 12.8 to 40.8%, rapid switching between plus- and minus end–directed ES was readily observed, similar to control cells (Fig. 7, A and B). Within 2.6 s, single virus particles were frequently switching from +0.4 μm/s to −0.4 μm/s and vice versa, suggesting that stable MTs supported rapid bidirectional transport.

In a number of cultured cells, including polarized cells, MTs can be detached from the MTOC and may occur as migrating antiparallel structures with free minus and plus ends at steady-state conditions (Keating et al., 1997). We therefore tested if the rapid switching between minus- and plus end–directed motions of wt Ad2 occurred near the MTOC in TC7/MAP4/MTB–GFP cells that were reestablishing MTs after nocodazole wash out. Such cells are expected to have a minimal amount of MTs that are not anchored to the MTOC. As indicated in Fig. 7 C, a perinuclear MT aster formed after 1–2 min of nocodazole wash out. MTOC-near viruses were observed to switch between plus- and minus end–directed motions at ES of 0.3–0.4 μm/s as indicated by a typical particle trace (Fig. 7 C). Although these amplitudes were somewhat smaller than those in the control or the taxol-treated cells, they were significantly larger than the randomly directed mean ES in nocodazole-treated HeLa (0.15 and 0.17 μm/s, Table I) or TC7 cells (data not shown). We thus concluded that single cytosolic Ad2 particles were able to engage with both plus- and minus end–directed motors and thus move bidirectionally along not highly dynamic MTs.

Dynein/Dynactin Significantly Contributes to Minus End–directed Transport of Cytosolic Ad2

The major minus end–directed motor complex of inter-

Table II. Significant Differences between Mean Speeds of Cytosolic Wt Ad2 or Endosomal Mutant Virus Ts1 (One-sided t test at the 95% Confidence Level, $\mu_1 < \mu_2$)

	μ_1		μ_2	
Periphery				
WtAd				
	HeLa	Noc	HeLa	No drug
				GFP
				DynGFP
	HeLa	Surface	HeLa	Noc
	TC7/MAP4-GFP	No drug	TC7 Contr	No drug
	TC7/MAP4-GFP	Surface	TC7/MAP4-GFP	No drug
			TC7 Contr	No drug
			HeLa	Noc
Ts1Ad	TC7/MAP4-GFP	No drug	TC7 Contr	No drug
			TC7/MAP4-GFP	Tax
MTOC				
WtAd				
	HeLa	No drug	TC7 Contr	No drug
			TC7/MAP4-GFP	No drug
			TC7/MAP4-GFP	Tax
	HeLa	GFP	TC7/MAP4-GFP	No drug
	HeLa	DynGFP	HeLa	No drug
			HeLa	GFP
			TC7 Contr	No drug
	HeLa	Noc	HeLa	DynGFP
	HeLa	Surface	HeLa	Noc
	TC7/MAP4-GFP	Surface	TC7 Contr	No drug
			TC7/MAP4-GFP	No drug
			HeLa	Noc

phase cells is cytoplasmic dynein (Vallee and Sheetz, 1996; Hirokawa, 1998). The motor activity can be experimentally dislodged from cargo by overexpression of p50/dynamitin, a component of the dynein-associated dynactin complex (Echeverri et al., 1996; Burkhardt et al., 1997; Ahmad et al., 1998). We therefore tested if transient overexpression of human dynamitin in HeLa cells affected nuclear targeting of Ad2. Control cells transfected with eGFP-encoding plasmid DNA showed efficient nuclear targeting of TR-labeled Ad2 at 60 min p.i. (Fig. 8 A, panels a–c). HeLa cells cotransfected with GFP and dynamitin plasmids showed reduced nuclear targeting of Ad2, particularly at high levels of overexpression (Fig. 7 A, panels d–f). At moderate dynamitin overexpressions, variable levels of nuclear targeting occurred, perhaps due to incomplete inactivation of the dynactin complex.

To test if dynamitin overexpression interfered with Ad2 escape from endosomes, we assayed the release of cointernalized fluid-phase dextran-FITC from endosomes to the cytosol upon Ad2 infection in a qualitative assay, similar to the HRP assay described in Fig. 4 B. To reliably determine the endpoint distribution of the dextran we used a

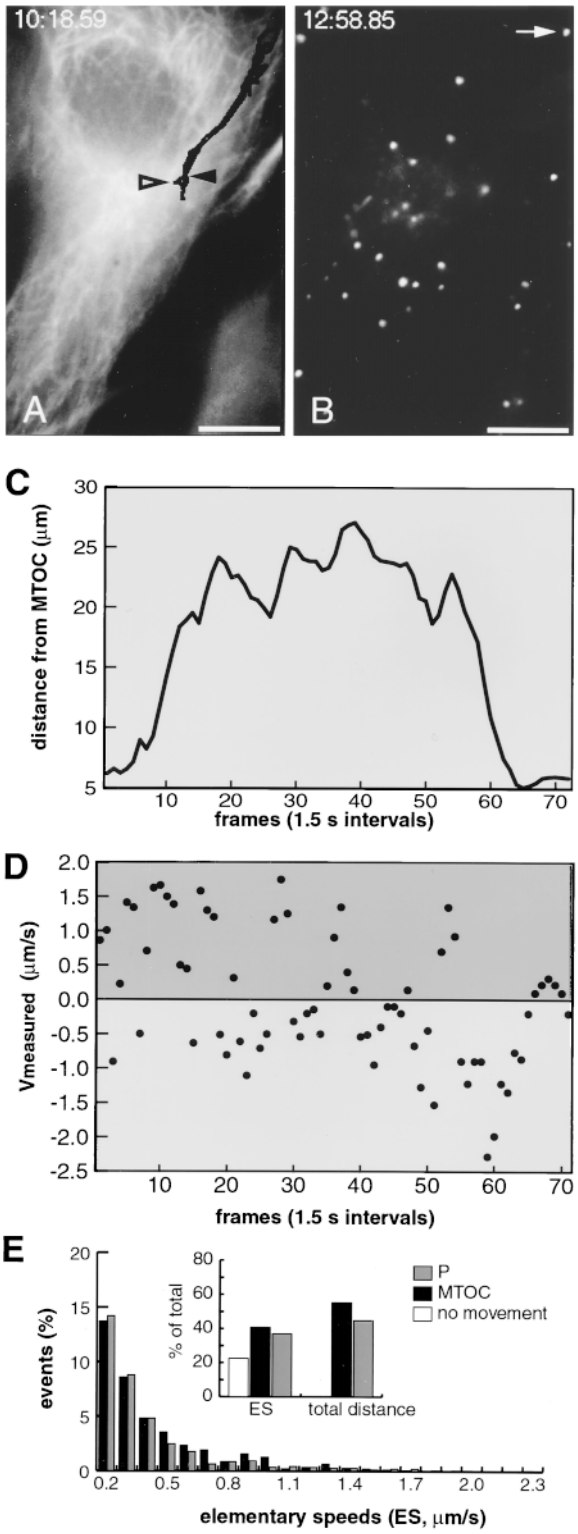

Figure 6. Fast minus- and plus end–directed transport of endosomal ts1 virus. TR-labeled ts1 virus was added to TC7/MAP4/MTB–GFP cells and TR images were recorded with intervals of 1.5 s starting 20 min p.i. The GFP signal at the beginning of the experiment is indicated in A and TR virus of frame 39 in panel B (time stamps indicating minutes:seconds.centiseconds). The first TR-frame was recorded 31.22 s after the initial GFP frame. One particular virus particle (white arrow in B) was followed in 72 subsequent frames as indicated by the black trace in A (white arrowhead indicating the particle position in frame 1 and black arrowhead indicating the position in frame 72). The particle distance to the presumptive MTOC is plotted in panel C and ES (μm/s) are indicated in D. (E) Population analysis of motile ts1 particles as described in Fig. 5 E (100% ES = 1,410, 100% distance = 754.2 μm). The corresponding movie is available at http://www.unizh.ch/~cellbio/jcb1999-1.html Bar, 10 μm.

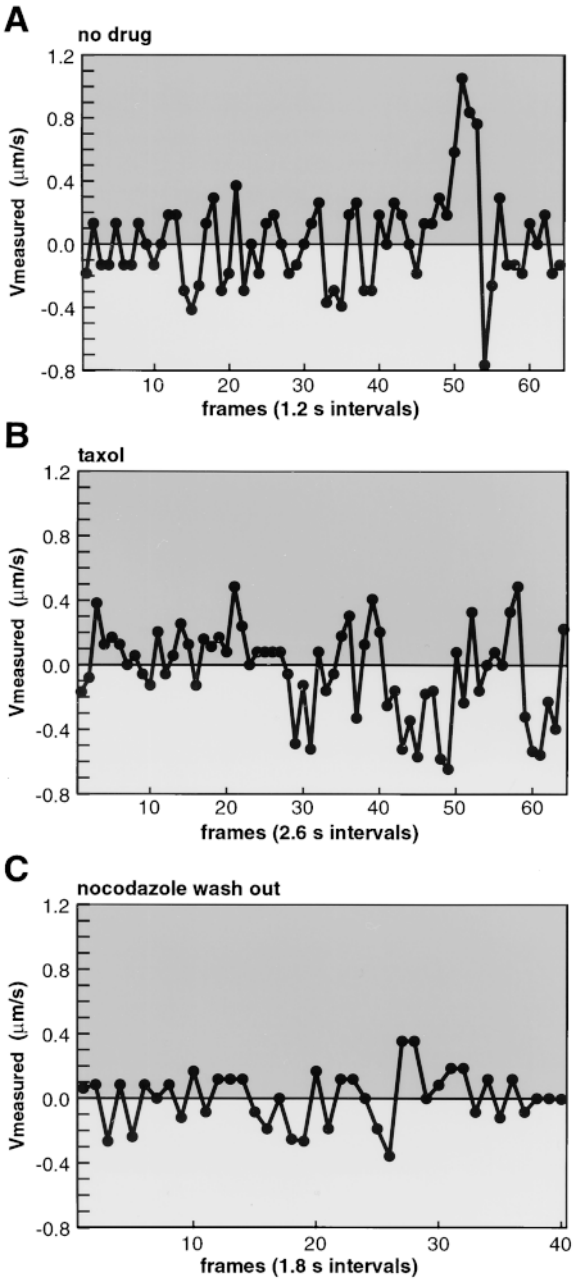

Figure 7. Rapid switching between minus- and plus end–directed motions of Ad2 wt in control nondrug-treated cells, taxol-treated TC7/MAP4/MTB–GFP cells, and also in cells reestablishing their MTs after nocodazole wash out. Ad2-TR was internalized for 20–40 min into TC7/MAP4-GFP cells not treated (A) or treated (B) with taxol (100 nM). Alternatively, cells were pretreated with nocodazole (20 μM) for 15 min in growth medium, incubated with Ad2-TR in cold binding medium in the presence of nocodazole for 60 min, followed by virus internalization for 30 min in the presence of nocodazole and 1–2 min after removal of the drug (C). Time-lapse micrographs were recorded as described in Materials and Methods and directional ES plotted against time. Representative traces of one particle for each condition are shown. Movies are available at http://www.unizh.ch/~cellbio/jcb1999-1.html

lysine-fixable 10-kD dextran, which readily diffuses from the cytosol to the nucleus. Wt Ad2 and, as a control, the mutant ts1 were bound to control cells or cells overexpressing dynamitin and internalized in the presence of dextran for 15 min, followed by a 15-min chase in the absence of dextran. About 80% of the cells infected with wt virus showed a prominent diffuse dextran pattern in the cytosol and the nucleus, independent of dynamitin overexpression (Fig. 8 B, panels a–c). Similar results were obtained with a control plasmid overexpressing the loop 1 region of the hexon protein (see Materials and Methods) (data not shown). In contrast, none of the more than 200 analyzed cells infected with ts1 virus showed any diffuse cytoplasmic or nuclear dextran staining, but contained numerous punctuate FITC signals in the cytoplasm indicative of endosomes or lysosomes (Fig. 8 B, panels d–f). These results were in full agreement with the HRP fluid-phase uptake experiments (Fig. 4 B) and suggested that dynamitin overexpression did not appreciably affect Ad2 release from endosomes.

To quantitate the effects of dynamitin overexpression on Ad2 trafficking, we compared the extents and frequencies of the minus and plus end–directed ES in dynamitin overexpressing HeLa cells with control and nocodazole-treated cells. Virus motility at the cell surface was, in addition, determined to account for cytosol-independent particle motion. As shown by an ES population analysis (Fig. 9 B) and exemplified by representative particle traces (Fig. 9 A), dynamitin overexpression significantly reduced the extents and also the frequencies of the minus end–directed ES. The mean minus end–directed speed of 0.22 μm/s was significantly smaller than the plus end–directed mean speed of 0.30 μm/s (Tables I and II), resulting in a plus end–directed population speed of 0.06 μm/s compared with a minus end–directed speed of 0.03 μm/s in control cells (Fig. 9 B, panels a and b) (Table I). As pointed out earlier, not all minus end–directed transport of Ad2 was blocked by dynamitin overexpression. This was illustrated also by the maximal minus end–directed ES (~2 μm/s) and a mean minus end speed, which was significantly higher than in nocodazole-treated cells (Table II). This result may either reflect the heterogenous expression levels of dynamitin or, alternatively, indicate some form of dynein/dynactin-independent minus end transport of Ad2. In contrast to the effect of dynamitin on the minus end migration of Ad2, dynamitin overexpression did not significantly affect the mean plus end–directed velocity, as illustrated by the predominantly peripheral virus localization in these cells (Fig. 8 A and Fig. 9 A, panel b_2) (Tables I and II). However, dynamitin overexpression significantly increased the frequency of plus end motions to 31.5 from 25.5% in control cells or 25.8% in GFP-expressing cells (legend of Table I, chi square test at 95% confidence). Interestingly, dynamitin overexpression also significantly increased the fraction of immobile particles to 50.9 from 41.4% in control cells. The validity of our chi square analysis and of the sample volumes were confirmed by the fact that there were no significant differencies between the plus, the minus, and the no movement frequencies in control HeLa cells compared with GFP-expressing HeLa cells. That the expression of GFP had no significant effects on Ad2 trafficking was further supported by the observa-

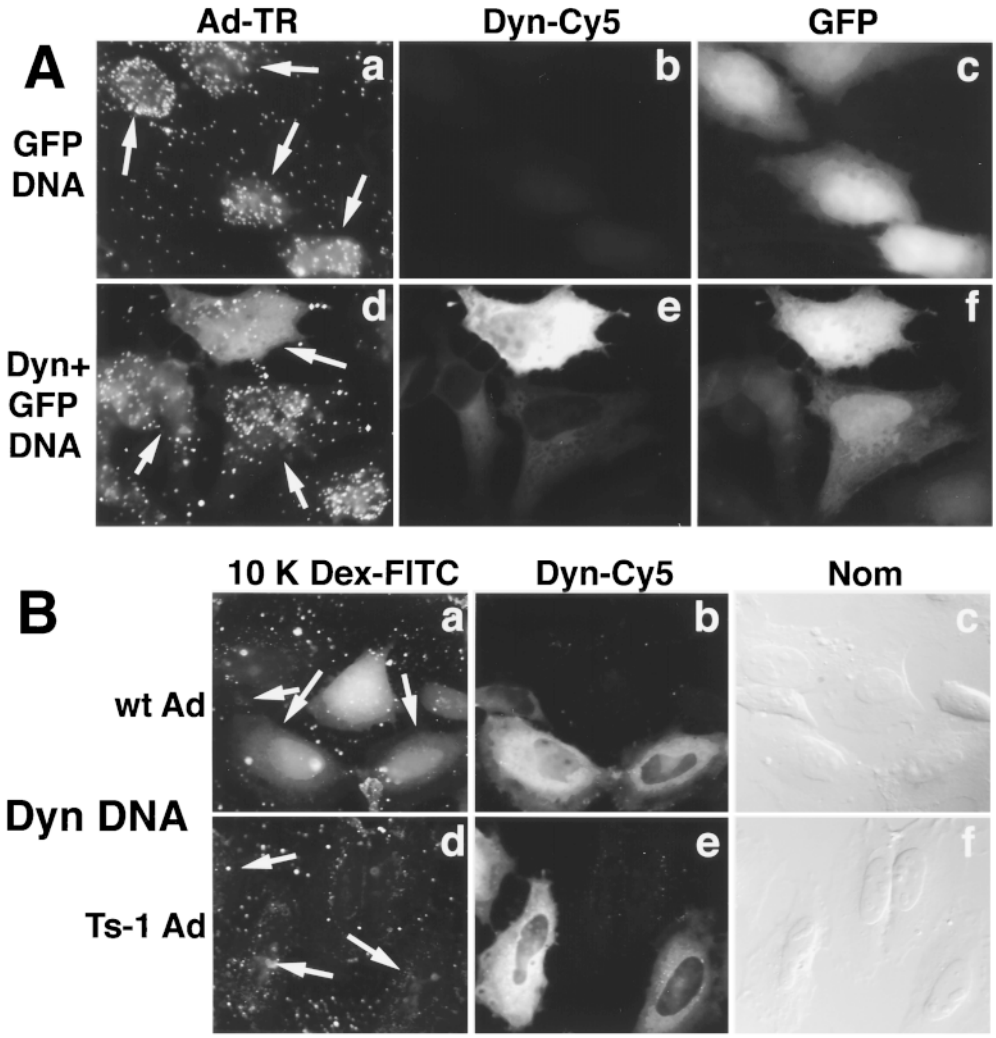

Figure 8. Dynamitin overexpression inhibits nuclear targeting of incoming Ad2, but not release of a fluid-phase endosomal marker into the cytosol. (A) TR-labeled wt virus was bound in the cold to HeLa cells transiently transfected with a plasmid DNA expressing eGFP (panels a–c, arrows) or with the eGFP-plasmid together with a dynamitin/p50 (Dyn)-expressing plasmid (panels d–f). In the latter case, 95% of the GFP expressing cells also overexpressed dynamitin. Virus was internalized for 60 min at 37°C and cells were processed for indirect immunofluorescence microscopy using anti-dynamitin mAb 50.1 and goat anti–mouse IgG-Cy5. (B) wt Ad2 (panels a–c) or ts1 (panels d–f) was bound at 50 μg/ml to the surface of HeLa cells, which had been transiently transfected with dynamitin/p50 DNA. Virus was internalized for 15 min in the presence of FITC-labeled 10 K dextran (5 mg/ml), followed by a 15-min incubation in the absence of dextran, fixed with pFA, and then stained for dynamitin using mAb 50.1 and anti-mouse IgG-Cy5 (panels b and e). The distribution of dextran was recorded in the FITC channel (panels a and d, transfected cells are indicated by an arrow) and DIC images of the same cells shown in panels c and f.

tion that the mean minus- and plus end–directed speeds were identical in GFP-expressing cells and control cells (Tables I and II, one-sided *t* test, 95% confidence).

Taken together, the data show that dynamitin overexpression strongly affected but not completely blocked minus end–directed transport of cytosolic Ad2. It increased the frequency of plus end movements and supported long-range movements over several micrometers towards the periphery. In contrast, no long-range movements, either MTOC- or periphery-directed, were observed in nocodazole-treated cells. In these cells, short-range random movements (covering areas of 5–10 μm^2) with mean speeds of 0.15 μm/s were observed (Fig. 9 A, panel c) (Table I). The motilities in nocodazole-treated cells were apparently randomly directed without any significant difference between plus- and minus end–directed mean speeds (Table II). These motilities were, however, not an artefact of our experimental set up, since they were significantly larger than the motilities of surface-bound virus (Fig. 9, A and B, panels d) (Table I). Possibly, in nocodazole-treated cells viruses were either moving on short MT fragments resistant to the drug, or they were using some MT-independent form of intracellular motility.

Discussion

In this study we have analyzed the dynamic properties of incoming Ad2 at various stages of entry. Our results identify the major minus end–directed motor complex, dynein/dynactin, as a key mediator of nuclear targeting of Ad2. The data support the notion that the viral DNA remains wrapped by the capsid until arrival at the nuclear membrane. Capsids therefore are expected to contain all the necessary information for nuclear targeting. Virus particles on the cell surface remain apparently immobile, probably bound to a primary receptor (Bergelson et al., 1997).

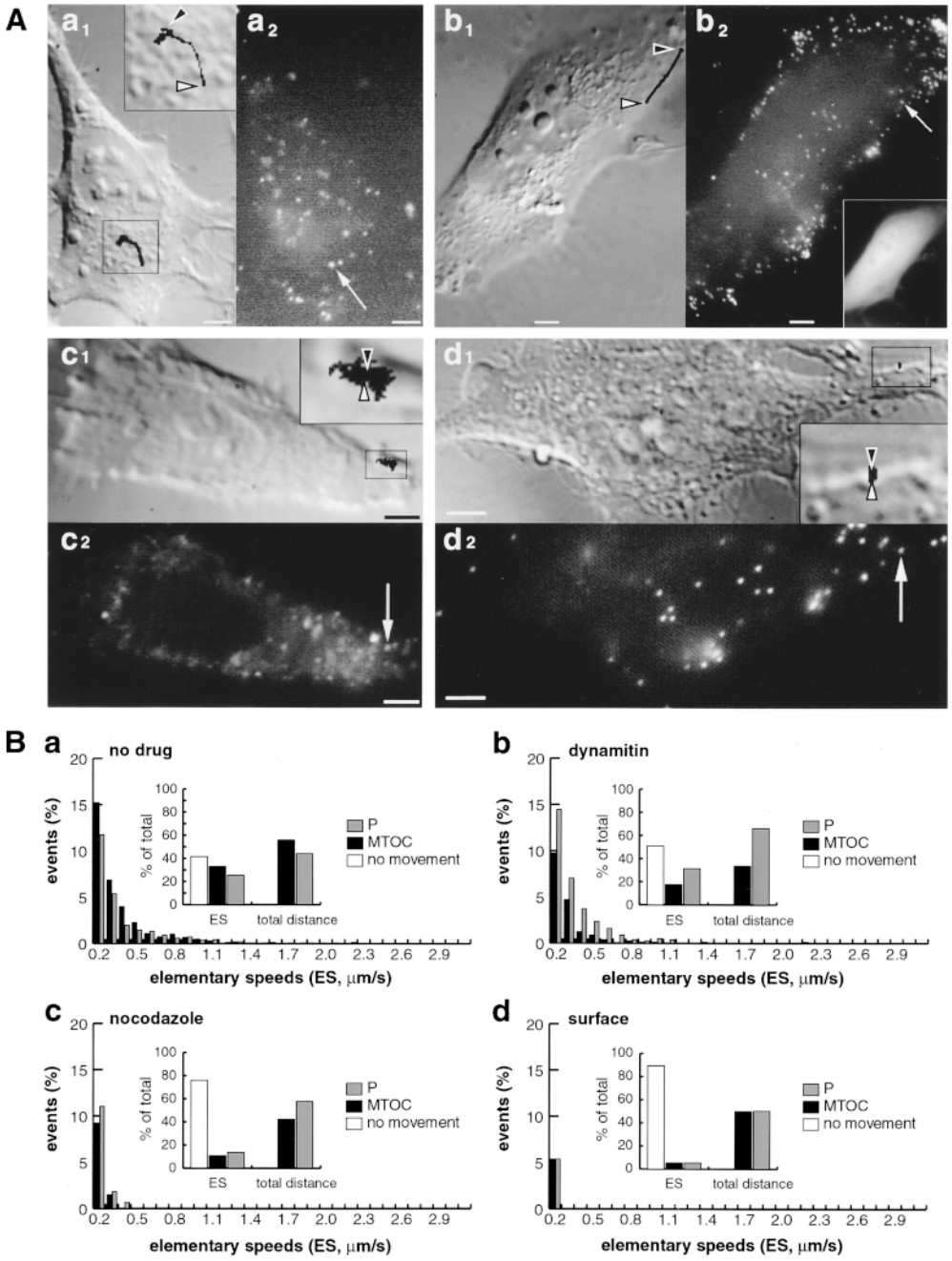

Figure 9. Dynamic analysis of wt Ad2 trafficking in HeLa cells overexpressing dynamitin and comparison to control, nocodazole-treated HeLa cells, and virus at the cell surface. Virus motilities in control HeLa cells (panels Aa and Ba, 40 min p.i.), HeLa cells overexpressing dynamitin (panels Ab and Bb, 40 min p.i.), cells treated with nocodazole (panels Ac and Bc, 40 min p.i.), and on the cell surface (panel Ad and Bd, 5 min p.i.) were measured as described in Fig. 5 A. Traces of a representative particle are shown for each condition in panel A merged onto a DIC image taken at the beginning of the TR recordings (shown in a_1, b_1, c_1, and d_1). The particle traces are derived from (a) 43 frames at 2.6-s intervals, (b) 37 frames at 2.1-s intervals, (c) 246 frames at 1.5-s intervals, and (d) 97 frames at 2.6-s intervals. Note that in the early stages of infection (panels d_1 and d_2), highly motile particles were occasionally seen moving towards the nucleus with micrometer per second speeds (see movie available at http://www.unizh.ch/~cellbio/jcb1999-1.html). These fast-moving particles may be contained in an endocytic vesicle or had just reached the cytosol. B shows cumulative distributions of ES for each of the conditions as described in Fig. 5. In panel Ba, 100% ES = 1,677, 100% distance = 721.4 μm; panel Bb 100% ES = 810, 100% distance = 244.9 μm; panel Bc, 100% ES = 608, 100% distance = 40.6 μm; panel Bd, 100% ES = 448, 100% distance = 11.5 μm. Movies are available at http://www.unizh.ch/~cellbio/jcb1999-1.html Bar, 5 μm.

They are then captured into endosomes, penetrate the endosomal membrane, and then move as naked cytosolic particles along MTs to the MTOC. Our dynamic analysis at a resolution of up to one frame per second shows that minus end migration occurs stepwise with maximal ES of 2.6 μm/s, occasionally interrupted by periods of almost equally fast plus end–directed motions or periods of stalling. Consequently, the population speeds towards the MTOC are in the order of micrometers per minute, in agreement with the observation that wt virus starts to accumulate at the MTOC and the nuclear envelope at 30–40 min p.i. In contrast to wt virus, the endosomal escape-defective mutant virus ts1 does not end up near the perinuclear MTOC, but remains randomly distributed in the cytoplasm, despite the fact that it undergoes fast minus- and plus end–directed elementary motion steps.

Cytosolic, but Not Endosomal Virus, Is Transported to the MTOC

Several lines of evidence indicate that cytosolic rather than endosomal viruses are transported to the MTOC. First, MT depolymerization with nocodazole effectively inhibited wt virus transport to the nuclear envelope and left capsids in the cytosol. These cytosolic capsids contain genomic DNA and are competent to translocate to the nuclear envelope and release their DNA into the nucleus if MTs are restored. Interestingly, microinjected viral DNA core structures lacking the remainder capsid components were not imported into the nucleus, but instead remained aggregated in the cytoplasm (data not shown). These results show that cytosolic capsid structures and intact MTs are of functional importance to nuclear import of viral DNA.

The second evidence favoring transport of naked rather than endosomal viruses to the MTOC is based on the different dynamic properties of wt virus compared with the endosomal ts1 mutant. Whereas wt Ad2 moves predominantly to the MTOC with population mean speeds between 0.03 and 0.21 μm/s (depending on the cell type), plus- and minus end–directed movements occur with about equal frequencies and extents in the case of the mutant ts1. Ts1-positive vesicles contain fluid-phase endocytic markers, such as HRP or fluorescent dextran indicating that they were of endocytic origin. Unlike transferrin-containing endosomes (Daro et al., 1996) ts1 did not accumulate near the MTOC within 60 min p.i., suggesting that the ts1 vesicles are perhaps routed towards lysosomes rather than a perinuclear recycling compartment. In accordance with this possibility, ts1 was degraded in a lysosomal protease-dependent manner starting at ~60 min p.i. (Greber et al., 1996). MTs are, however, involved in ts1 trafficking, since nocodazole largely inhibited long-range ts1 movements (data not shown). Like in the case of wt virus, dynamic MTs are not required for ts1 motility. Elimination of the most dynamic MTs by taxol not only increased the mean minus- and plus end–directed speeds of ts1, but also increased the frequency of no movements, thus supporting the notion that dynamic MTs may facilitate establishing MT contact with cargo (Goodson et al., 1997).

The Nature of Ad2 Movements through the Cytosol

The analysis of intracellular wt virus dynamics in nondrug-treated cells shows that between 12.8 and 41.4% of the elementary motion steps were less than 0.1 μm/s depending on the cell line. This was below the resolution of our set up and was therefore scored as no movement. Almost all the particles were, however, closely associated with MTs as suggested by confocal microscopy and earlier EM studies (data not shown) (Luftig and Weihing, 1975; Weatherbee et al., 1977; Miles et al., 1980). It is therefore possible that cytosolic virus first attaches to MTs and remains immobile until some motor-dependent transport happens. Transport to the MT minus ends (or to a lesser extent also the plus ends) occurred by two types of motion, a slow transport mode working at micrometers per minute and a fast mode working at micrometers per second. Both modes are made up of numerous ES with peak speeds in the order of 0.5–2.6 μm/s. The fast mode is reminiscent of vesicular trafficking (Presley et al., 1998) and typically lasted for several seconds resulting in efficient virus advancement to the MTOC. It is not interrupted by stalling or plus end–directed motions. Unlike the fast mode, the slow mode can last for minutes and is composed of alternating minus- and plus end–directed ES, which are typically less than 0.5 μm/s in magnitude. Since these motions often follow a quasi-linear track and are completely eliminated in the presence of nocodazole, they are most likely mediated by MT-dependent motors.

Rapid switching between plus- and minus end–directed motions is not only detected in nondrug-treated cells, but also in taxol-incubated cells and, importantly, in cells recovering from nocodazole treatment immediately after drug wash out. In the latter case, most of the MTs that were not anchored to the MTOC, including antiparallel MTs, are expected to be eliminated (Keating et al., 1997). We therefore concluded that a single Ad2 particle engages with both plus- and minus end–directed motor activities. The ability to use both types of motors might be important for Ad entry into polarized cells or, possibly, for virus egress from infected polarized or nonpolarized cells. Whether, and if so, how the motor activities are coordinated is subject of future studies. Besides motor regulation, MTs and associated proteins could have a potential role in determinating the directionality of transport. Interestingly, both the mean and also the peak periphery-directed speeds of wt Ad2 and endosomal mutant virus were significantly decreased in cells overexpressing the MT-binding domain of MAP4 compared with the parental cells. Whether this effect is related to the observed increase in MT stability in the MAP4/MTB–GFP–expressing cells (Nguyen et al., 1997) is not known.

MT-dependent transport of cargo can, in principle, be driven by the energetics of plus end MT depolymerization and dynamic attachment of the motor to the shortening filament (Waters and Salmon, 1996). Our data with taxol-stabilized MTs show that highly dynamic MTs are not required for long-range Ad2 transport. Dynamic MTs may, however, increase the probability of virus contact with MTs, since taxol strongly increased the fraction of nonmotile viruses.

Dynein/Dynactin Is a Major Minus End–directed Motor for Ad2

Like other MT-based motors, the major minus end–directed motor dynein produces directed movement by a conformational change upon ATP-hydrolysis (Howard, 1997; Hirokawa, 1998; Hirokawa et al., 1998). Dynein is a protein complex of three different subunits of various stoichiometries translocating along MTs at speeds faster than 0.5 μm/s (Schroer, 1996). Dynein attaches to cargo, such as cellular vesicles and mitotic chromosomes via the dynactin complex. Overexpression of the dynactin component dynamitin has been shown to disrupt the dynactin complex on the kinetochore of mitotic chromosomes (Echeverri et al., 1996) and also affect vesicular trafficking in interphase cells (Burkhardt et al., 1997; Ahmad et al., 1998). Our results show that overexpression of human dynamitin significantly inhibits nuclear targeting of Ad2 in HeLa cells and,

to a lesser extent, also in monkey TC7 cells (data not shown). It is unlikely that dynamitin overexpression inhibited Ad2 penetration, since a fluid-phase endocytic marker is delivered to the cytosol upon Ad2 infection, independent of dynamitin overexpression. Accordingly, general receptor-mediated endocytic uptake is known to occur without intact MTs (Gruenberg et al., 1989; Rickard and Kreis, 1996). Although not all minus end–directed transport of wt virus was blocked in the presence of excess dynamitin, our data imply that some component of the dynactin complex directly or indirectly interacts with cytosolic Ad2 capsid. Owing to the linearity of the remaining minus end–directed movements, this motility is unlikely caused by Brownian motion (Beckerle and Porter, 1982). It rather reflects either some dynein/dynactin-independent, but MT-dependent motor activity or, possibly, the heterogenous expression levels of dynamitin (Burkhardt et al., 1997). Interestingly, dynamitin overexpression significantly increased the frequencies of no movements and of plus end–directed movements, which could suggest that a plus end–directed motor attaches to a site on the virus or even on a dynactin component, which is normally occupied by dynein/dynactin (Blangy et al., 1997).

With the advent of increasingly detailed models of motor interactions with MTs for kinesin (Woehlke et al., 1997) and dynein (Gee et al., 1997) and increasing structural understanding of kinesin's directionality (Case et al., 1997; Henningsen and Schliwa, 1997), a more detailed knowledge of the mechanism of dynein motor directionality and interactions with simple cargo is desired. We already know much about the cell biology of motors involved in vesicular transport, such as dynein's role in trafficking of the intermediate compartment (Presley et al., 1997), Golgi vesicles (Fath et al., 1997; Holleran et al., 1998; Lippincott-Schwartz, 1998; Vaisberg et al., 1996), mature phagosomes (Blocker et al., 1997), and endosomes (Aniento et al., 1993; Goodson et al., 1997), but we know very little about MT-dependent trafficking of nonmembranous organelles or of viral structures. Owing to its relative simplicity and high entry efficiency, Ad offers yet another opportunity to get additional insights into the complex regulation of polarized cytoplasmic trafficking. In addition, any successful application of gene transfer protocols requires overcoming of numerous subcellular barriers including the cytoplasm. Our present study, together with a recent report on Herpes virus (Sodeik et al., 1997), indicates that DNA viruses can overcome the cytoplasmic barrier by packaging their genomes into a capsid structure, which is capable of using the minus end–directed MT-dependent dynein motor.

Our present study is the first dynamic and functional analysis of an incoming viral structure. It demonstrates that individual Ad2 particles engage not only with a minus end–directed motor for DNA delivery into the nucleus, but also interact with a fast plus end–directed activity working at micrometer per second speeds. In HeLa and TC7 cells, the plus end–directed motions are of lower efficiency than the minus end motions, allowing nuclear targeting of virus at population speeds in the order of micrometers per minute. It is likely that long-range cytoplasmic motility of nucleic acids generally requires some form of active transport as demonstrated also for mRNAs in oocytes (Bassell and Singer, 1997; Grünert and St. Johnston, 1996). For optimal efficiency of future synthetic or semisynthetic nucleic acid delivery systems viral and/or cellular elements may therefore be used to facilitate directional movement through the cytoplasm.

We thank T. Bächi, J. Bulinski, P. Draber, L. Gerace, T. Kreis, J.C. Perriard, B. Sodeik (Medizinische Hochschule, Hanover, Germany), and R. Vallee for valuable discussions, antibodies, plasmid DNA, or cell lines. T. Bächi is acknowledged for allowing access to the laser scanning confocal microscope at the Laboratory for Electron Microscopy of the University of Zürich (Zürich, Switzerland).

This work was supported by a grant from the Swiss National Science Foundation to U.F. Greber, a European Molecular Biological Organization long-term fellowship to M. Suomalainen, and the Kanton of Zürich.

Received for publication 21 July 1998 and in revised form 4 January 1999.

References

Ahmad, F.J., C.J. Echeverri, R.B. Vallee, and P.W. Baas. 1998. Cytoplasmic dynein and dynactin are required for the transport Of microtubules into the axon. *J. Cell Biol.* 140:391–401.

Aniento, F., N. Emans, G. Griffiths, and J. Gruenberg. 1993. Cytoplasmic dynein-dependent vesicular transport from early to late endosomes. *J. Cell Biol.* 123:1373–1387.

Auerbach, D., B. Rothen-Ruthishauser, S. Bantle, M. Leu, E. Ehler, D. Helfman, and J.C. Perriard. 1997. Molecular mechanisms of myofibril assembly in heart. *Cell Struct. Funct.* 22:139–146.

Bassell, G., and R.H. Singer. 1997. mRNA and cytoskeletal filaments. *Curr. Opin. Cell Biol.* 9:109–115.

Beckerle, M.C., and K.R. Porter. 1982. Inhibitors of dynein activity block intracellular transport in erythrophores. *Nature*. 295:701–703.

Bergelson, J.M., J.A. Cunningham, G. Droguett, E.A. Kurt-Jones, A. Krithivas, J.S. Hong, M.S. Horwitz, R.L. Crowell, and R.W. Finberg. 1997. Isolation of a common receptor for Coxsackie B viruses and adenoviruses 2 and 5. *Science*. 275:1320–1323.

Blangy, A., L. Arnaud, and E.A. Nigg. 1997. Phosphorylation by p34cdc2 protein kinase regulates binding of the kinesin-related motor HsEg5 to the dynactin subunit p150. *J. Biol. Chem.* 272:19418–19424.

Blocker, A., F.F. Severin, J.K. Burkhardt, J.B. Bingham, H. Yu, J.C. Olivo, T.A. Schroer, A.A. Hyman, and G. Griffiths. 1997. Molecular requirements for bi-directional movement of phagosomes along microtubules. *J. Cell Biol.* 137:113–129.

Bulinski, J.C., T.E. McGraw, D. Gruber, H.L. Nguyen, and M.P. Sheetz. 1997. Overexpression of Map4 inhibits organelle motility and trafficking in vivo. *J. Cell Sci.* 110:3055–3064.

Burkhardt, J.K., C.J. Echeverri, T. Nilsson, and R.B. Vallee. 1997. Overexpression of the dynamitin (p50) subunit of the dynactin complex disrupts dynein-dependent maintenance of membrane organelle distribution. *J. Cell Biol.* 139:469–484.

Burnett, R.M. 1997. The structure of adenovirus. *In* Structural Biology of Viruses. W. Chiu, R.M. Burnett, and R.L. Garcea, editors. Oxford Press, Oxford, UK. 209–238.

Case, R.B., D.W. Pierce, N. Hom-Booher, C.L. Hart, and R.D. Vale. 1997. The directional preference of kinesin motors is specified by an element outside of the motor catalytic domain. *Cell*. 90:959–966.

Cole, D.G., D.R. Diener, A.L. Himelblau, P.L. Beech, J.C. Fuster, and J.L. Rosenbaum. 1998. *Chlamydomonas* kinesin-II-dependent intraflagellar transport (IFT): IFT particles contain proteins required for ciliary assembly in *Caenorhabditis elegans* sensory neurons. *J. Cell Biol.* 141:993–1008.

Cudmore, S., I. Reckmann, and M. Way. 1997. Viral manipulations of the actin cytoskeleton. *Trends Microbiol.* 5:142–148.

Dales, S., and Y. Chardonnet. 1973. Early events in the interaction of adenoviruses with HeLa cells. IV. Association with microtubules and the nuclear pore complex during vectorial movement of the inoculum. *Virology.* 56:465–483.

Daro, E., P. van der Sluijs, T. Galli, and I. Mellman. 1996. Rab4 and cellubrevin define different early endosome populations on the pathway of transferrin receptor recycling. *Proc. Natl. Acad. Sci. USA*. 93:9559–9564.

Desai, A., and T.J. Mitchison. 1997. Microtubule polymerization dynamics. *Ann. Rev. Cell Dev. Biol.* 13:83–117.

Doxsey, S.J., J. Sambrook, A. Helenius, and J. White. 1985. An efficient method for introducing macromolecules into living cells. *J. Cell Biol.* 101:19–27.

Echeverri, C.J., B.M. Paschal, K.T. Vaughan, and R.B. Vallee. 1996. Molecular characterization of the 50-kD subunit of dynactin reveals function for the complex in chromosome alignment and spindle organization during mitosis. *J. Cell Biol.* 132:617–633.

Fath, K.R., G.M. Trimbur, and D.R. Burgess. 1997. Molecular motors and a spectrin matrix associate with Golgi membranes in vitro. *J. Cell Biol.* 139: 1169–1181.

Gee, M.A., J.E. Heuser, and R.B. Vallee. 1997. An extended microtubule-binding structure within the dynein motor domain. *Nature*. 390:636–639.
Georgi, A., C. Mottola-Hartshorn, A. Warner, B. Fields, and L.B. Chen. 1990. Detection of individual fluorescently labeled reovirions in living cells. *Proc. Natl. Acad. Sci. USA*. 87:6579–6583.
Ghadge, G.D., R.P. Roos, U.J. Kang, R. Wollmann, P.S. Fishman, A.M. Kalynych, E. Barr, and J.M. Leiden. 1995. CNS gene delivery by retrograde transport of recombinant replication-defective adenoviruses. *Gene Ther*. 2:132–137.
Goodson, H.V., C. Valetti, and T.E. Kreis. 1997. Motors and membrane traffick. *Curr. Opin. Cell Biol.* 9:18–28.
Greber, U.F. 1998a. Delivery of animal virus DNA into the nucleus. *In* Self-assembling Complexes for Gene Delivery: From Chemistry to Clinical Trial. L. Seymour, A. Kabanov, and P. Felgner, editors. John Wiley & Sons, Sussex, UK. 89–114.
Greber, U.F. 1998b. Virus assembly and disassembly: the adenovirus cysteine protease as a trigger factor. *Rev. Med. Virol.* 8:213–222.
Greber, U.F., M. Willetts, P. Webster, and A. Helenius. 1993. Stepwise dismantling of adenovirus 2 during entry into cells. *Cell*. 75:477–486.
Greber, U.F., P. Webster, J. Weber, and A. Helenius. 1996. The role of the adenovirus protease in virus entry into cells. *EMBO (Eur. Mol. Biol. Organ.) J*. 15:1766–1777.
Greber, U.F., M. Suomalainen, R.P. Stidwill, K. Boucke, M. Ebersold, and A. Helenius. 1997. The role of the nuclear pore complex in adenovirus DNA entry. *EMBO (Eur. Mol. Biol. Organ.) J*. 16:5998–6007.
Greber, U.F., M.Y. Nakano, and M. Suomalainen. 1998. Adenovirus entry into cells: a quantitative fluorescence microscopy approach. *In* Adenovirus Methods and Protocols. Methods Mol. Med. Vol 21. W.S.M. Wold, editor. Humana Press, Totowa, NJ. 217–230.
Gruenberg, J., G. Griffiths, and K.E. Howell. 1989. Characterization of the early endosome and putative endocytic carrier vesicles in vivo and with an assay of vesicle fusion in vitro. *J. Cell Biol.* 108:1301–1316.
Grünert, S., and D. St. Johnston. 1996. RNA localization and the development of asymmetry during *Drosophila* oogenesis. *Curr. Opin. Gen. Dev*. 6:395–402.
Grussenmeyer, T., K.H. Scheidtmann, M.A. Hutchinson, W. Eckhart, and G. Walter. 1985. Complexes of polyoma virus medium T antigen and cellular proteins. *Proc. Natl. Acad. Sci. USA*. 82:7952–7954.
Henningsen, U., and M. Schliwa. 1997. Reversal in the direction of movement of a molecular motor. *Nature*. 389:93–96.
Hirokawa, N. 1998. Kinesin and dynein superfamily proteins and the mechanism of organelle transport. *Science*. 279:519–526.
Hirokawa, N., Y. Noda, and Y. Okada. 1998. Kinesin and dynein superfamily proteins in organelle transport and cell division. *Curr. Opin. Cell Biol.* 10:60–73.
Holleran, E.A., S. Karki, and E.L. Holzbaur. 1998. The role of the dynactin complex in intracellular motility. *Int. Rev. Cytol*. 182:69–109.
Horwitz, M.S. 1990. Adenoviruses. *In* Virology. Vol. 1. B.N. Fields and D.M. Knipe, editors. Raven Press, New York. 1723–1740.
Howard, J. 1997. Molecular motors: structural adaptations to cellular functions. *Nature*. 398:561–567.
Hoyt, M.A., A.A. Hyman, and M. Bahler. 1997. Motor proteins of the eukaryotic cytoskeleton. *Proc. Natl. Acad. Sci. USA*. 94:12747–12748.
Ireton, K., and P. Cossart. 1997. Host-pathogen interactions during entry and actin-based movement of *Listeria* monocytogenes. *Annu. Rev. Genet*. 31: 113–138.
Keating, T.J., J.G. Peloquin, V.I. Rodionov, D. Momcilovic, and G.G. Borisy. 1997. Microtubule release from the centrosome. *Proc. Natl. Acad. Sci. USA*. 94:5078–5083.
Komiyama, M., T. Soldati, P. von Arx, and J.C. Perriard. 1996. The intracompartmental sorting of myosin alkali light chain isoproteins reflects the sequence of developmental expression as determined by double epitope-tagging competition. *J. Cell Sci*. 109:2089–2099.
Kreis, T.E. 1987. Microtubules containing detyrosinated tubulin are less dynamic. *EMBO (Eur. Mol. Biol. Organ.) J*. 6:2597–2606.
Leopold, P.L., B. Ferris, I. Grinberg, S. Worgall, N.R. Hackett, and R.G. Crystal. 1998. Fluorescent virions—dynamic tracking of the pathway of adenoviral gene transfer vectors in living cells. *Hum. Gene Ther*. 9:367–378.
Liao, G., T. Nagasaki, and G.G. Gundersen. 1995. Low concentrations of nocodazole interfere with fibroblast locomotion without significantly affecting microtubule level: implications for the role of dynamic microtubules in cell locomotion. *J. Cell Sci.* 108:3473–3483.
Lippincott-Schwartz, J. 1998. Cytoskeletal proteins and Golgi dynamics. *Curr. Opin. Cell Biol*. 10:52–59.
Luby-Phelps, K. 1994. Physical properties of the cytoplasm. *Curr. Opin. Cell Biol.* 6:3–9.
Luftig, R.B., and R.R. Weihing. 1975. Adenovirus binds to rat brain microtubules in vitro. *J. Virol.* 16:696–706.
Mandelkow, E., and E.M. Mandelkow. 1995. Microtubules and microtubule-associated proteins. *Curr. Opin. Cell Biol*. 7:72–81.
Mermall, V., P.L. Post, and M.S. Mooseker. 1998. Unconventional myosins in cell movement, membrane traffic, and signal transduction. *Science*. 279: 527–533.
Miles, B.D., R.B. Luftig, J.A. Weatherbee, R.R. Weihing, and J. Weber. 1980. Quantitation of the interaction between adenovirus types 2 and 5 and microtubules inside infected cells. *Virol.* 105:265–269.
Moudjou, M., N. Bordes, M. Paintrand, and M. Bornens. 1996. γ-Tubulin in mammalian cells: the centrosomal and the cytosolic forms. *J. Cell Sci*. 109: 875–887.
Nguyen, H.L., S. Chari, D. Gruber, C.M. Lue, S.J. Chapin, and J.C. Bulinski. 1997. Overexpression of full- or partial length Map4 stabilizes microtubules and alters cell growth. *J. Cell Sci.* 110:281–294.
Novakova, M., E. Draberova, W. Schurmann, G. Czihak, V. Viklicky, and P. Draber. 1996. γ Tubulin redistribution in taxol-treated mitotic cells probed by monoclonal antibodies. *Cell Motil. Cytoskel.* 33:38–51.
Olson, K.R., J.R. McIntosh, and J.B. Olmsted. 1995. Analysis of MAP 4 function in living cells using green fluorescent protein (GFP) chimeras. *J. Cell Biol*. 130:639–650.
Pazour, G.J., C.G. Wilkerson, and G.B. Witman. 1998. A dynein light chain is essential for the retrograde particle movement of intraflagellar transport (IFT). *J. Cell Biol*. 141:979–992.
Prchla, E., C. Plank, E. Wagner, D. Blaas, and R. Fuchs. 1995. Virus-mediated release of endosomal content in vitro: different behavior of adenovirus and rhinovirus serotype 2. *J. Cell Biol.* 131:111–123.
Presley, J.F., N.B. Cole, T.A. Schroer, K. Hirschberg, K.J. Zaal, and J. Lippincott-Schwartz. 1997. ER-to-Golgi transport visualized in living cells. *Nature*. 389:81–85.
Presley, J., C. Smith, K. Hirschberg, C. Miller, N. Cole, K. Zaal, and J. Lippincott-Schwartz. 1998. Golgi membrane dynamics. *Mol. Biol. Cell*. 9:1617–1626.
Rickard, J.E., and T.E. Kreis. 1996. Clips for organelle–microtubule interactions. *Trends Cell Biol*. 6:178–183.
Ridoux, V., J.J. Robert, X. Zhang, M. Perricaudet, J. Mallet, and G. Le Gal La Salle. 1994. Adenoviral vectors as functional retrograde neuronal tracers. *Brain Res*. 648:171–175.
Schroer, T.A. 1996. Structure and function of dynactin. *Semin. Cell Dev. Biol*. 7:321–328.
Seksek, O., J. Biwersi, and A.S. Verkman. 1997. Translational diffusion of macromolecule-sized solutes in cytoplasm and nucleus. *J. Cell Biol.* 138:131–142.
Shenk, T. 1996. Adenoviridae. *In* Fundamental Virology. B.N. Fields, D.M. Knipe, and P.M. Howley, editors. Lippincott-Raven, New York. 979–1016.
Sodeik, B., M.W. Ebersold, and A. Helenius. 1997. Microtubule-mediated transport of incoming Herpes Simplex Virus 1 capsids to the nucleus. *J. Cell Biol*. 136:1007–1021.
Vaisberg, E.A., P.M. Grissom, and J.R. McIntosh. 1996. Mammalian cells express three distinct dynein heavy chains that are localized to different cytoplasmic organelles. *J. Cell Biol*. 133:831–842.
Vale, R.D., and R.J. Fletterick. 1997. The design plan of kinesin motors. *Annu. Rev. Cell Dev. Biol.* 13:745–777.
Vallee, R.B., and M.P. Sheetz. 1996. Targeting of motor proteins. *Science*. 271: 1539–1544.
Waterman-Storer, C.M., and E.D. Salmon. 1997. Actomyosin-based retrograde flow of microtubules in the lamella of migrating epithelial cells influences microtubule dynamic instability and turnover and is associated with microtubule breakage and treadmilling. *J. Cell Biol*. 139:417–434.
Waters, J.C., and E.D. Salmon. 1996. Cytoskeleton: a catastrophic kinesin. *Curr. Biol*. 6:361–363.
Weatherbee, J.A., R.B. Luftig, and R.R. Weihing. 1977. Binding of adenovirus to microtubules. II. Depletion of high-molecular-weight microtubule-associated protein content reduces specificity of in vitro binding. *J. Virol.* 21:732–742.
Weber, J.M. 1995. The adenovirus endopeptidase and its role in virus infection. *In* Molecular Repertoire of Adenoviruses. W. Doerfler and P. Böhm, editors. Springer, Berlin, Germany. 227–235.
Welch, M.D., A. Mallavarapu, J. Rosenblatt, and T.J. Mitchison. 1997. Actin dynamics in vivo. *Curr. Opin. Cell Biol*. 9:54–61.
Whittaker, G.R., and A. Helenius. 1998. Nuclear import and export of viruses and virus genomes. *Virology*. 246:1–23.
Woehlke, G., A.K. Ruby, C.L. Hart, B. Ly, N. Hombooher, and R.D. Vale. 1997. Microtubule interaction site of the kinesin motor. *Cell*. 90:207–216.